Mathematical Biosciences and Engineering

http://www.aimspress.com/journal/mbe

MBE, 23(2): 388–420.
DOI: 10.3934/mbe.2026016
Received: 16 September 2025
Revised: 22 October 2025
Accepted: 28 October 2025
Published: 07 January 2026

Research article

Qualitative optimization of oncolytic virotherapy and immune therapy combination treatments

Negar Mohammadnejad and Thomas Hillen*

Department of Mathematical and Statistical Sciences, University of Alberta, 116 St & 85 Ave, Edmonton, T6G 2R3, Canada

* **Correspondence:** Email: thillen@ualberta.ca.

Abstract: Oncolytic viruses (OVs) are designed to selectively target and destroy cancer cells while sparing normal, healthy tissue. Several viruses for oncolytic virotherapy are currently developed. In this paper, we will use mathematical modeling to consider key strategies that can improve the efficacy of oncolytic virotherapy. These include the integration of immunotherapy approaches with virotherapy to amplify anti-tumor immune responses, as well as optimizing the timing, dosage, and sequencing of viral administrations. Specifically, we consider strategies that increase the burst size of the virus, immunostimulation and immunosuppression, we optimize for different weekly virus injection schedules, and we consider the combination of OV therapy with chimeric antigen receptor (CAR) T-cell therapy. A limiting factor is the availability of data. We parametrize the model using several different data sets. These, however, correspond to different cancers and experimental setups. Hence our model cannot be considered to be validated. Consequently, our results are qualitative. Our results highlight the critical importance of timing for virotherapy's efficacy and overall success. They outline strong evidence for promising treatment scenarios that needs to be further tested experimentally in the future.

Keywords: virotherapy; immunotherapy; cancer modelling; optimized schedule; oncolytic virus

1. Introduction

The mechanism of oncolytic viruses (OVs) is similar to that of conventional viruses; they enter the host cells and exploit the cell's genetic machinery to replicate and spread [1–3]. What distinguishes OVs is their capacity to selectively target and destroy cancer cells while sparing normal, healthy tissue. The immune system was once considered a limiting factor, with the belief that its response to the virus would inhibit replication, restrict viral spread, and reduce tumor cell killing. However, this view has largely shifted, as it is now recognized that the immune system plays a pivotal role in OV–cancer interactions [4,5]. Viral infection of the tumor enhances its visibility to the immune system, promoting

recognition and attack [4, 6, 7]. Moreover, virus-induced lysis of tumor cells leads to the release of tumor antigens into a microenvironment modified by infection, thus reversing tumor-induced immune suppression. The first genetically engineered OV, a herpes simplex virus 1 (HSV-1) mutant with deficient thymidine kinase, was developed in 1991 and used to treat malignant glioma in nude mice [8]. These viruses preferentially target and eliminate cancer cells, often leveraging dendritic cells to mediate their effects [6].

Baadbdulla et al. [9] extensively studied a mathematical model for the temporal and spatial interactions of the virus and the cancer cells without considering the effect of the immune system. In the absence of OVs, tumors are known to create an immunosuppressive environment, effectively silencing the body's immune response against cancer cells. However, once oncolytic viruses are introduced, they induce pro-inflammatory signaling within the tumor microenvironment. This shift not only weakens the tumor's defenses but also enhances its susceptibility to immunotherapies. Oncolytic virotherapy (OVT) awakens the immune system, enabling a robust response against the tumor. Therefore, incorporating the immune system into the model is essential. It is important to note that the oncolytic virus may be cleared from the body before treatment can fully eliminate the tumor. Despite the fact that OVs were translated into clinical trials, with talimogene laherparepvec (T-VEC) receiving U.S. Food and Drug Administration (FDA) approval for melanoma, there are still challenges, such as limited viral infection and immune clearance, that need to be overcome [7].

Based on the model of Al-Tuwairqi et al. [10], we incorporate the population of immune cells into a model and build a base model, which investigates the fundamental interactions of immune response with cancer and with the oncolytic virus. In [10], the authors conducted a qualitative analysis of the model and its steady states. They examined the existence and stability of equilibrium points, and through numerical analysis they found oscillatory behavior. Moreover, they demonstrate the impact of various parameters on treatment outcomes. We continue this research by including specific OV treatment strategies and combination treatments. Specifically, we analyze the outcome of an increased effective viral production rate, the effect of immuno-suppression and immuno-stimulation, we optimize the scheduling of OV injections, and we combine OV therapy with chimeric antigen receptor (CAR) T-cell therapy.

We find an important aspect of combination therapies, which is often forgotten in theoretical or experimental studies, the timing of the treatments. Using our oncolytic virus model, we show that the efficacy of treatment can be significantly boosted compared to the traditional dosing, when a massively different timing is applied. In our case, optimal schedules gives an initial dose on day one, and additional, larger doses in the following weeks. We obtained that the outcome of the treatment is significantly more successful when the virotherapy is re-administered three or four weeks after treatment began. The sensitive dependence of the treatment outcome on the scheduling is surprising, and offers a simple way to improve these treatments.

After exploring various treatment variations, we extended our analysis of the OVT base models in appendix B by incorporating a more specific representation of immune responses and analyzing the same treatments within this enhanced framework. We find essentially the same results as the more complex model. Also in this case, a careful treatment scheduling of viral injections makes a huge difference in the model outcome.

It needs to be pointed out that our work has not been validated against data and results that we have obtained in this work should not be considered as treatment recommendations. Our results are

quantitative. They outline strong evidence for promising treatment scenarios that need to be further tested experimentally in the future.

1.1. Previous modeling of OV therapy

There is a considerable history of mathematical modeling of oncolytic virotherapy. The works by Baabdulla et al. [9] and Al-Tuwairqi et al. [10], mentioned earlier, build on this foundation. One of the earliest models was introduced in 2001 by Wodarz [11]. His proposed model explored how virotherapy could be optimized to achieve maximal therapeutic effects. Wodarz examined three main mechanisms of action: direct viral killing of tumor cells, immune responses against the virus that indirectly aid therapy, and the induction of tumor-specific immune responses triggered by the infection. The analysis demonstrated that simply increasing the virus's cytotoxicity is not always beneficial, as overly rapid killing can limit virus spread and reduce treatment efficacy. Instead, an optimal balance must be struck between viral replication and cytotoxicity. Building on this, in 2009 Komarova and Wodarz [12] presented a broader modeling framework that accounted for different modes of virus spread (fast vs. slow) and tumor growth kinetics. Their key insight was that the dynamics of OV therapy can fall into two qualitatively distinct regimes, the fast spread and the slow spread. In the following year, in [13], they continued their study of the OVT dynamics and developed a general system of ordinary differential equations (ODEs) that builds on biologically motivated properties of tumor growth and viral spread. They analyzed how varying these assumptions would alter system dynamics and defined conditions under which virus-mediated tumor eradication would be possible. Their work also underscored the importance of model robustness and cautioned that many classical modeling results may be artifacts of arbitrary mathematical choices. Their work on oncolytic virotherapy has served as a foundational framework upon which more complex models have been constructed.

In 2011, Tian [14] introduced a model comprising of three variables, the uninfected and infected cancer cells, and the virus and his analysis showed the burst size of the oncolytic virus plays a crucial role in the success of virotherapy. His findings underscored the importance of optimizing the burst size of oncolytic viruses in virotherapy. In the other studies of the OVT, the focus was on the role of the immune system in the cancer-virus interactions. In the work done by Eftimie et al. [15], a detailed ODE-based model with two compartments (lymphoid and peripheral) was developed to represent interactions between uninfected/infected tumor cells, memory/effector immune cells, and the two viruses-adenovirus (Ad) vaccine and an oncolytic vesicular stomatitis virus (VSV). This model could accurately reproduce the experimental tumor dynamics and immune responses. Using this mathematical model, they explored the conditions necessary for achieving permanent tumor elimination. They had their focus on two complex dynamic behaviors: multi-stability and multi-instability. Their work also identified that the prolonged oncolytic virus presence is lined to a distinct phenomenon—multi-instability. Additionally, they assessed whether viral persistence alone was sufficient for tumor elimination. The findings revealed that without an active anti-tumor immune response, even a sustained anti-viral effect could not prevent tumor growth. Thus, successful treatment requires the combined action of both immune-mediated tumor killing and oncolytic viral activity. In another study on the immune-virus interactions, Storey et al. [16] distinguished between the innate and adaptive (tumor and virus specific) immune response. They pointed out that the innate immune system clears the virus too quickly, reducing its ability to infect tumor cells and stimulate an effective antitumor immune response and as a result, OVT alone is often insufficient for tumor clearance. They modeled a combination ther-

apy of OVT and the protein 1/programmed death-ligand 1 (PD-1/PD-L1) checkpoint inhibitor. This combination therapy prevents T-cell exhaustion, improves immune-mediated tumor killing, and significantly lowers the viral infectivity threshold required for successful treatment. They highlighted the importance of careful scheduling and dosing in combination therapy. Their analysis pointed out that administering a second viral dose too soon after the first can worsen treatment outcome due to immune system redirection toward viral rather than tumor antigens.

In 2021, Pooladvand et al. [17] developed a 3D spatiotemporal model to study the dynamics of cancer-virus interactions, specifically focusing on adenovirus therapy within a solid tumor. In their study, by linking partial differential equation (PDE) modeling with bifurcation analysis, they revealed deep insights into why virotherapy often falls short as a standalone treatment, and underlined the limitations of virotherapy as a monotherapy. They also highlighted the need for combination strategies to achieve complete tumor control.

2. The basic OV-immune mathematical model

Our model for immune response to oncolytic virotherapy is based on a standard oncolytic virus model as analyzed recently in Baabdulla [9]. This model is well known in the literature and has been used in many publications [10,11,14,17]. Their model considers three populations: uninfected cancer cells $C(t)$, infected cancer cells $I(t)$, and free virus particles $V(t)$. Here, we extend this framework to incorporate the immune response. The most straightforward way to include immunity in the system is by introducing a population of effector immune cells $Y(t)$, following the approach of Al-Tuwairqi et al. [10]. We make two minor modifications to the model studied in [10], resulting in the following space-independent system:

$$\begin{aligned}
\frac{dC}{dt} &= rC\left(1-\frac{C+I}{L}\right)-\beta CV-p_1YC,\\
\frac{dI}{dt} &= \beta CV-\alpha I-q_1YI,\\
\frac{dV}{dt} &= \alpha bI-\omega V-s_1VY,\\
\frac{dY}{dt} &= \eta_1YC+\zeta_1YI-\xi_1Y,
\end{aligned} \tag{2.1}$$

where $Y(t)$ represents the population of immune cells.

The first equation describes the logistic growth of uninfected cancer cells at rate r, with carrying capacity L, and their infection by virus particles at rate β. The second equation accounts for the formation of infected cancer cells through infection and their subsequent lysis at rate α. The third equation models the production of free viruses from lysed infected cells, where b is the viral burst size and ω is the viral clearance rate.

The interactions between the immune system and the other populations are represented by standard mass-action terms: p_1, q_1, and s_1 denote the rates of immune-mediated killing of uninfected cancer cells, infected cancer cells, and viruses, respectively. The last equation describes the stimulation and proliferation of immune cells by both uninfected and infected cancer cells, with stimulation rates η_1 and ζ_1. Immune cells are cleared at rate ξ_1. From this point forward, we will refer to system (2.1) as our base model.

In contrast, the model proposed by Al-Tuwairqi et al. [10] included a viral loss term of the form $-\beta_2 CV$ in the virus equation. However, several studies [9, 11, 15, 18] have argued that such a term can be neglected, as viral infection typically has a negligible effect on the total viral population. For this reason, we omit this term here. Additionally, we do not include a natural cancer cell death term, $-dC$, in the C-equation, since on the short time scale relevant to OV therapy (a few weeks), this effect is minimal. Additionally, choosing the natural death rate of cancer to be zero corresponds to the worst case scenario, and it is expected that good treatment will do well if such a term would be included.

In Figure 1(a),(b), we sketch the interactions of the elements of the Baadbulla et al. model from [9], and our onco-virus-immune base model (2.1), respectively.

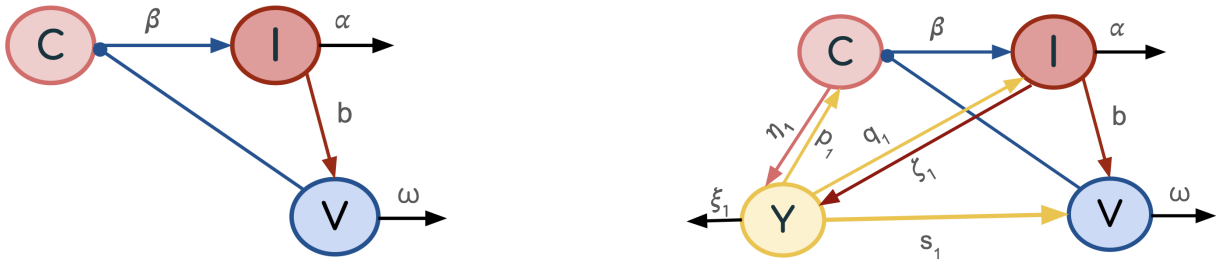

(a) **(b)**

Figure 1. (a) The blue arrows represent the viral infection of cancer cells at rate β. The red arrows indicate the burst of viruses released from lysed infected cells at rate b. All black arrows depict cell death and virus degradation (b) The blue and black arrows represent similar dynamics as in (a). The yellow arrows indicate cell and virus death by the immune system at rates p_1, q_1, and s_1 respectively. The pink arrow shows immune stimulation by uninfected cancer cells, while the red arrow shows stimulation by infected cancer cells.

We consider the system (2.1) with the initial conditions:

$$C(0) = N_0 > 0, \quad I(0) = I_0 = 0, \quad V(0) = V_0 > 0, \quad Y(0) = Y_0 > 0.$$

The values of the initial conditions are presented in Table 1.

Table 1. Initial conditions for model variables.

Variable	Value	Unit	Description
C_0	10^6	cells/mm^3	Initial density of uninfected cells
I_0	0	cells/mm^3	Initial density of infected cells
V_0	1.9×10^{10}	virons/mm^3	Initial density of virus particles
Y_0	10^4	units/mm^3	Initial density of immune cells

We choose parameter values based on previous studies. Pooladvand et al. [17] considered the carrying capacity of a solid tumor of radius 1 mm is about $L = 10^6$ cells per mm^3; this value is based on Lodish [19]. We consider this value as the initial density of uninfected tumor cells, N_0, in our model. Based on the experiments by Kim et al. [20] on adenovirus in the glioblastoma U343 cell line, the tumor

growth rate was estimated to be approximately 0.3 per day. This value was also adopted by Baabdulla et al. [9] in their model. The initial condition for the amount of adenovirus virions is $V_0 = 1.9 \times 10^{10}$ virions per mm^3. We also adopt the same parameter values for L, β, ω, and b as those used in the model by Baabdulla et al. [9]. These parameters are associated with a reovirus and were applied in the context of breast cancer. For the remaining parameters, we use estimates based on the immune-virotherapy interaction model developed by Al-Tuwairqi et al. [10]. In their study, these parameters were examined in the context of glioma treatment. The virus-related parameters in their model were derived from the study by Friedman et al. [21], which focused on the mutant herpes simplex virus 1 (hrR3). Al-Tuwairqi's immune model [10] incorporated components of the innate immune response, including natural killer cells and cytokine activity. We summarize the model parameters in Table 2, and for completeness, we report the parameter values of the cited papers in Appendix A, Table A1.

Table 2. Parameters for the base model (2.1), their baseline values, and their references.

Parameter	Description	Baseline value	Units	Source
r	Growth rate of uninfected tumor	0.3	$(\text{day})^{-1}$	[9]
L	Tumor carrying capacity	10^6 ($10^6 - 10^8$)	cells	[9]
β	Infection rate of uninfected tumor cells by OV	1.5×10^{-9}	$(\text{virus}\cdot\text{day})^{-1}$	[9]
p_1	Killing rate of tumor by immune cells	0.48×10^{-6}	$(\text{cell}\cdot\text{day})^{-1}$	[10] (estimated)
α	Death rate of infected tumor cells	1	$(\text{day})^{-1}$	[9]
q_1	Killing rate of infected tumor by tumor-specific immune cells	0.63×10^{-6}	$(\text{cell}\cdot\text{day})^{-1}$	[10] (estimated)
b	Viruses released by lysed infected tumor cell	3500	$(\text{virus})(\text{cell})^{-1}$	[9]
ω	Virus-induced immune response rate	4	$(\text{day})^{-1}$	[9]
s_1	Killing rate of virus by immune cells	0.21×10^{-6}	$(\text{cell}\cdot\text{day})^{-1}$	[10] (estimated)
η_1	Stimulation of immune response by uninfected cells	3.84×10^{-7}	$(\text{cell}\cdot\text{day})^{-1}$	[10] (estimated)
ζ_1	Stimulation of immune response by infected cells	7.8×10^{-7}	$(\text{cel}\cdot\text{day})^{-1}$	[10] (estimated)
ξ_1	clearance rate of immune cells	0.036	$(\text{day})^{-1}$	[10]

To simplify our analysis, we apply the non-dimensionalization method by considering

$$\hat{C} = \frac{C}{L}, \quad \hat{I} = \frac{I}{L}, \quad \hat{V} = \frac{\beta V}{r}, \quad \hat{Y} = \frac{Y}{L}, \quad \hat{x} = x\sqrt{\frac{\tau}{D_V}}, \text{ and } \quad \hat{t} = \tau t.$$

The dimensional model (2.1) transforms into the nondimensional system:

$$\begin{aligned}
\frac{d\hat{C}}{d\hat{t}} &= \hat{C}\left(1 - \hat{C} - \hat{I}\right) - \hat{C}\hat{V} - p\hat{Y}\hat{C}, \\
\frac{d\hat{I}}{d\hat{t}} &= \hat{C}\hat{V} - a\hat{I} - q\hat{Y}\hat{I}, \\
\frac{d\hat{V}}{d\hat{t}} &= \theta\hat{I} - \gamma\hat{V} - s\hat{V}\hat{Y}, \\
\frac{d\hat{Y}}{d\hat{t}} &= \eta\hat{Y}\hat{C} + \zeta\hat{Y}\hat{I} - \xi\hat{Y},
\end{aligned} \tag{2.2}$$

where

$$p = \frac{p_1 L}{r}, \quad q = \frac{q_1 L}{r}, \quad s = \frac{s_1 L}{r} \quad a = \frac{\alpha}{r}, \quad \theta = \frac{\alpha b \beta L}{r^2}, \quad \gamma = \frac{\omega}{r}, \quad \eta = \frac{\eta_1 L}{r}, \tag{2.3}$$

$$\zeta = \frac{\zeta_1 L}{r}, \quad \xi = \frac{\xi_1}{r}.$$

The parameter values before and after non-dimentionalization are given in Tables 2 and 3, respectively.

Table 3. Parameters for the base model (2.1) and their baseline values after non-dimensianlization (2.3).

Parameter	Description	Baseline value
θ	Effective viral production rate	58.33 (16.6–500)
p	Killing rate of tumor by immune cells	1.6
q	Killing rate of infected tumor by tumor-specific immune cells	2.1
γ	Virus clearance rate	13.33
s	Killing rate of virus by immune cells	0.71
η	Stimulation of immune response by uninfected cells	1.28
ζ	Stimulation of immune response by infected cells	2.6
ξ	clearance rate of immune cells	0.16

Note that we solve (2.2) numerically using MATLAB's built-in ODE solvers (`ode45` or `ode23`), and rescale the results into dimensional variables so that densities and time are presented in their physical units.

3. Analysis of the base model

The base model (2.1), in the absence of immune cells, was analyzed by Baabdulla et al. [9]. Their analysis showed that, under the baseline parameters, the system settles at a coexistence equilibrium, indicating that OVT alone would not be sufficient for tumor eradication. They also noted that while their mathematical results were insightful, predictions beyond the first few days are not realistic due to the eventual activation of the immune system. Before analyzing the full model, we should note that the immune system alone is often insufficient to eradicate tumors because many cancers develop immunosuppressive microenvironments that prevent effective immune recognition and attack. As described in [22], oncolytic viruses can overcome this limitation by "heating up" otherwise immunologically "cold" tumors. In the context of our model, this biological mechanism directly affects the immune stimulation rate parameter, η, which captures the enhanced activation and recruitment of immune effector cells in response to viral therapy.

Now, we consider the full system and here we summarize the basic dynamical properties of model (2.2). A complete analysis of the model is presented in [5]. Model (2.2) has the following equilibria:

trivial $E_0 = (0,0,0,0)$	cancer only $E_1 = (1,0,0,0)$	immune free $E_2 = \left(\frac{a\gamma}{\theta}, \frac{-a\gamma+\gamma\theta}{\theta(\gamma+\theta)}, \frac{-a\gamma+\theta}{\gamma+\theta}, 0\right)$
cancer-immune $E_3 = \left(\frac{\xi}{\eta}, 0, 0, \frac{1-\frac{\xi}{\eta}}{p}\right)$		coexistence $E_4 = \left(\hat{C}_4, \hat{I}_4, \hat{V}_4, \hat{Y}_4\right)$

where E_4 is the coexistence point which cannot be expressed explicitly.

In [5], we prove the following theorem.

Theorem 1. *For our base immune-oncolytic virus model* (2.2)*, we have the following results. The basic reproduction number is given by* $R_0 = \dfrac{\theta}{a\gamma}$*. E_0 is always a saddle, and when the basic reproduction*

number R_0 is less than one, E_1 is locally asymptotically stable and E_2 is not biologically relevant. When R_0 is greater than one, E_1 becomes unstable and the coexistence steady state arises through a transcritical bifurcation at $\theta_t = a\gamma$, where E_2 becomes biologically relevant. E_2 is locally asymptotically stable when

$$\theta > \frac{\gamma\left(\zeta + \eta a - \xi\right) + \gamma\sqrt{\left(\zeta + \eta a - \xi\right)^2 + 4a\xi(\zeta - \xi)}}{2\xi}, \tag{3.1}$$

and

$$\theta > \theta_t = a\gamma \quad \textit{and} \quad \kappa(\theta) > 0, \tag{3.2}$$

where

$$\kappa(\theta) = -\theta^3 + m\theta^2 + \gamma m\theta + a\gamma^3, \quad \textit{and} \quad m = (a+\gamma)^2 + a(\gamma + 1).$$

There exists a bifurcation value $\theta_H > \theta_t$ with $\kappa(\theta_H) = 0$ such that the system undergoes a **Hopf bifurcation** *at E_2. E_3 is locally asymptotically stable only if we have*

$$\frac{\eta}{\xi}\left(a + q\left(\frac{1 - \frac{\xi}{\eta}}{p}\right)\right)\left(\gamma + s\left(\frac{1 - \frac{\xi}{\eta}}{p}\right)\right) > \theta. \tag{3.3}$$

For parameter values beyond the Hopf bifurcation point ($\theta > \theta_H$), the system exhibits strong oscillatory dynamics characterized by sharp bursts of viral activity followed by extended quiescent phases during which the tumor regrows. Despite these fluctuations, the cancer population repeatedly drops to very low levels between oscillations, which can be interpreted as a favorable therapeutic outcome. To quantitatively assess the overall treatment efficacy, we evaluate the tumor control probability (TCP) as a measure of long-term tumor suppression.

3.1. Tumor control probability

To effectively compare treatment strategies and better estimate their expected success, we need a suitable metric. Traditionally, TCP has been used in radiotherapy as a measure of the likelihood that treatment has successfully eliminated all clonogenic cells. In the study by Gong et al. [23], the Poisson-based TCP was identified as a reasonable first-order approximation for comparing the effectiveness of different treatment protocols. The Poissonian TCP is based on a stochastic process for the random variable X_t of viable cancer cells at time t. Assuming that individual cell deaths occur independently and that survival events are rare, X_t can be approximated by a Poisson distribution. We have that under a Poisson distribution with the expectation of λ events in a given interval, the probability of k tumor cells surviving is given by [24].

$$P(X = k) = \frac{\lambda^k e^{-\lambda}}{k!}. \tag{3.4}$$

If N_0 denotes the initial number of tumor cells and $S(t)$ the surviving fraction at time t, then the expected number of surviving cells is given by $E(X_t) = \lambda$. Approximating this expectation by $N_0 S(t)$, we obtain $\lambda = N_0 S(t)$. Consequently, the Poisson-based TCP is

$$TCP(t) = \Pr(X_t = 0) = e^{-N_0 S(t)}. \tag{3.5}$$

In our model (2.1), we normalize the cell density $C(t)$ with $L = N_0$. Hence, here the survival fraction is simply $S(t) = \dfrac{C(t)}{N_0} = \hat{C}(t)$. Therefore, our TCP is given by

$$TCP(t) = e^{-N_0\hat{C}(t)} = e^{-C(t)}. \tag{3.6}$$

In addition, we employ the area under the curve (AUC) as a quantitative measure of the total temporal effect of a treatment over a specified time period. This approach enables us to compare the temporal tumor control achieved under different parameter sets in a consistent and objective manner. A higher AUC indicates a more sustained TCP over time, whereas a lower AUC reflects less effective or shorter control. When comparing simulations with differing time horizons, the AUC is normalized by the total duration to yield an average TCP value, ensuring comparability across cases.

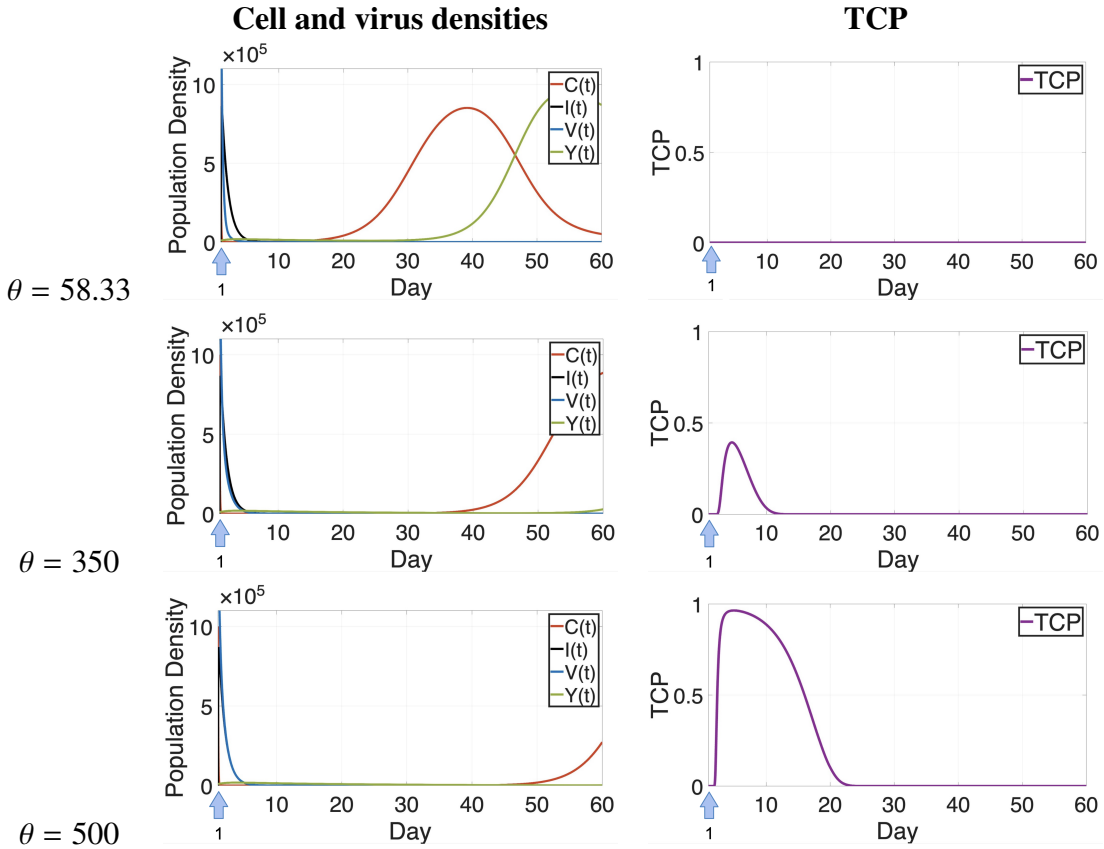

Figure 2. Strategy (S1): Dynamics of the cancer cells, virus, and immune cells of model (2.2) for a single dose of virus with different values of θ. The density of virus particles is re-scaled by dividing by 10^4. Note that we solve (2.2) numerically and rescale the results into dimensional variables so we can present densities and time in their physical units. The right column shows the corresponding TCP plots. The small blue arrow indicates the day of administration of the viral dose.

Overall, while the shape of the TCP curve captures transient effects in tumor dynamics, the AUC condenses this temporal behavior into a single scalar metric suitable for systematic comparison. Letting

TCP(t) denote the tumor control probability at time t, the normalized AUC over a time interval $[t_0, t_f]$ is defined as:

$$\text{Normalized AUC} = \frac{1}{t_f - t_0} \int_{t_0}^{t_f} \text{TCP}(t)\, dt. \tag{3.7}$$

We use our base value parameters from Table 3 to numerically solve system (2.2), and compute the cell densities, virus load, and TCP in the first row of Figure 2.

In our simulations, we introduce a cutoff threshold to regulate the viral load. Specifically, if at any time the viral concentration falls below 10^{-14}, it is considered cleared and is set to zero. This cutoff is applied because values below 10^{-14} correspond to a fraction of a virion, which is not biologically meaningful and should be treated as zero.

The plots of the base case in the first row of Figure 2 indicate a rapid initial decline in cancer cells when the OV is administered; however, the cancer cells quickly recover and approach their carrying capacity. Activated immune cells manage to reduce the population of cancer cells, but the tumor is not cleared. There is no signal in the TCP value throughout the base case, indicating that with these parameter values the OVT alone is not successful.

A sensitivity analysis of the parameters of this model was performed in [5], where it was observed that the success of OVT is strongly influenced by the virus effective proliferation rate and the immune-related parameters. In particular, the immune stimulation rate (η) and immune exhaustion rate (ξ) had the most pronounced effects on treatment outcome, while the viral production rate (θ) also played a significant, though comparatively smaller, role. These findings suggest that therapeutic strategies targeting these key parameters—enhancing immune stimulation, reducing immune exhaustion, and optimizing viral production—could substantially improve OVT efficacy.

4. Model strategies to improve treatment efficacy

We observed in the previous section, that the mathematical model predicting OVT as a monotherapy with one viral injection would not be successful. In this section, our goal is to use the model to discuss improved treatment strategies. We will refine our model, explore different parameter values, and test various combination therapies to achieve a more effective approach for cancer eradication. One of our key strategies will be combining virotherapy with immunotherapy, as this has been recognized as one of the most promising ways to enhance OVT efficacy. At the end of this section, we will compare all the results to gain a better understanding of how virotherapy can be optimized for more successful treatment outcomes. Our base model will be system (2.2), where Y is considered a general immune response which acts on both the virus and cancer cells. We will build upon this model by incorporating enhancements to improve treatment effectiveness. Here is a quick look at the strategies we will consider in the following:

(S1) Increasing the effective viral production rate θ. The parameter θ is a combined quantity (see (2.3)), which includes the viral binding rate β and the burst size b. Increasing either of these parameters increases θ.

(S2) Developing optimized daily and weekly dosing schedules for up to four weeks following the first viral injection.

(S3) Combining virotherapy with immunotherapy:

(a) Immunosuppression strategies

(b) Immune stimulation approaches

(c) Combination with CAR-T cell therapy, including optimized scheduling strategies.

4.1. Strategy (S1): Increase of viral production rate

The efficacy of the virus in eradicating cancer cells largely depends on its inherent properties, including the infection rate β and burst size b. Therefore, we will closely examine the parameter $\theta = \frac{\alpha b \beta L}{r^2}$ which incorporates both of these factors. In the estimations performed by [25], the burst size b of adenoviruses was found to range between 1000 and 100,000. In our simulations shown in Figure 2, we use the baseline parameter values from Table 2, where β was considered to be 3500, and thus, θ was set to 58.33. According to the findings in [25], the possible range for θ extends to over 1600. In this section, we investigate whether increasing the effective production rate has a positive impact on the outcome of OVT.

As it is seen in Figure 2, increasing θ value in model (2.2) is an effective approach to enhance the efficacy of OVT. The therapy becomes relatively successful, with the TCP curve approaching one, only when θ is nearly ten times higher than our baseline value. While this strategy significantly improves OVT's effectiveness and brings it closer to achieving complete cancer eradication, it is important to note that this value is currently out of reach for realistic viruses.

4.2. Strategy (S2): OVT schedule optimization

Related to the under performance of OVT, many have argued that lower doses distributed over several days, rather than the maximum tolerated dose, may be associated with improved tumor response [26–28]. In [27], Naumenko et al. pointed out that despite a lack of direct infection, subsequent viral doses—through a monocyte-dependent mechanism—enhance and sustain the infection initiated by the first dose. This process enhances $CD8^+$ T cell recruitment, delays tumor progression, and improves survival in multi-dosing OV therapy. These findings highlight the importance of dose optimization for the successful clinical development of OVT. Having an available mathematical model (2.2), we now address such a scheduling optimization. Our objective is to identify treatment schedules that minimize tumor load at the end of therapy, improving upon the results observed previously. The goal is to increase TCP values and maintain them at 1 for an extended period. To relate our theoretical treatment schedules to clinical practice, we refer to the recently published *International Virotherapy Association Guidelines on the Use of RIGVIR® in Oncology* (2024) [29]. These guidelines summarize protocols used in human virotherapy with the ECHO-7 oncolytic virus (RIGVIR®). The treatment is administered intramuscularly according to the *regional principle*, typically in muscles near major lymph node groups such as the deltoid or gluteal regions. The standard protocol is long-term (2–3 years) and consists of repeated injection cycles. For instance, in patients undergoing melanoma excision, three intramuscular injections are given on consecutive days around the primary site, starting 5–7 days before surgery and continuing postoperatively, followed by monthly or bimonthly injections for up to three years. After lymph node excision, the injections alternate between regions to stimulate different lymphatic areas. For patients with brain metastases, combined intramuscular and intranasal administrations are recommended to enhance delivery across the blood–brain barrier. Moreover, RIGVIR®

is often given between, but not concurrently with, chemotherapy or radiotherapy to avoid immune suppression while maintaining antiviral and antitumor activity.

Although our numerical protocol is simplified for modeling purposes, it is conceptually consistent with these clinical regimens: both involve periodic viral administrations designed to sustain viral activity, stimulate immune responses, and improve tumor control over extended periods rather than relying on a single high-dose treatment.

We incorporate a control term $u(t)$ into our model (2.2) to analyze treatment success. We test various dosing schedules with different viral dose levels. Our analysis considers treatment durations ranging from one week to five doses over a four-week period. A key constraint in our optimization is that the total dose administered each week must be equal to 95, which is equal to the initial value that was used by Baabdulla et al. [9]. Adding a control term $u(t)$ in the nondimensional model (2.2) gives

$$\begin{aligned} \frac{dC}{dt} &= C(1-C-I) - CV - pYC, \\ \frac{dI}{dt} &= CV - aI - qYI, \\ \frac{dV}{dt} &= \theta I - \gamma V - sVY + u(t), \\ \frac{dY}{dt} &= \eta YC + \zeta YI - \xi Y. \end{aligned} \tag{4.1}$$

We focus on treatment schedules that can be realistically implemented in clinical practice. Specifically, we allow at most one treatment per day and exclude treatments on weekends. We set the treatment to be performed in a period of 4 weeks or 28 days. However, it is important to note that the model (4.1) is nondimensionalized, and the nondimensional time $\hat{t}$ is defined by $\hat{t} = 0.3 \times t$. This implies that day 28 corresponds to $\hat{t} = 8.4$. Consequently, the objective function of this optimization problem is to minimize the uninfected tumor load $\hat{C}(\hat{t})$ at the end of the period ($\hat{t} = 8.4$). For simplicity, we will omit the hats from this point forward, with the understanding that all variables refer to their nondimensionalized form unless otherwise specified. We let N denote the total number of doses and S represent the schedule matrix. S has 4 rows and 5 columns. Each row stands for a week of therapy and each column corresponds to a day of the week. Since no therapy is performed on the weekends, we only consider 5 columns– Monday, Tuesday, Wednesday, Thursday, and Friday. The matrix S consists of *0's* and *1's*. We set an element of the matrix to be 1 if a dose of virus is administered on the corresponding day noting that we do not consider multiple doses on a single day. We also consider a matrix D with the same size as S, representing the value of dose given on the corresponding day. The *schedule matrix* S and the *dosage matrix* D can be written as

$$S = \begin{bmatrix} 1 & s_{12} & s_{13} & s_{14} & s_{15} \\ s_{21} & s_{22} & s_{23} & s_{24} & s_{25} \\ s_{31} & s_{32} & s_{33} & s_{34} & s_{35} \\ s_{41} & s_{42} & s_{43} & s_{44} & s_{45} \end{bmatrix}, \quad D = \begin{bmatrix} d_{11} & d_{12} & d_{13} & d_{14} & d_{15} \\ d_{21} & d_{22} & d_{23} & d_{24} & d_{25} \\ d_{31} & d_{32} & d_{33} & d_{34} & d_{35} \\ d_{41} & d_{42} & d_{43} & d_{44} & d_{45} \end{bmatrix}. \tag{4.2}$$

$$s_{ij} \in \{0, 1\}, \quad d_{ij} \in \mathbb{R}_+, \quad d_{ij} = 0 \text{ if } s_{ij} = 0. \tag{4.3}$$

The element (1, 1) is considered to be 1, since we assume that we always perform virotherapy on day 1, which in this version corresponds to $t = 0.3$. On treatment days ($s_{ij} = 1$) a treatment is given once with dose d_{ij}. Hence, we write out the treatment function as

$$u(t) = \sum_{i=1}^{4} \sum_{j=1}^{5} d_{ij} s_{ij} \delta_{t_{ij}}(t) \quad \text{where} \quad t_{ij} = 0.3 \times ((i-1) \times 7 + j) \tag{4.4}$$

and $\delta_{t_{ij}}(t)$ denotes the Dirac-delta distribution. The t_{ij} represents the days that the treatment is administered starting from 1 to 28. We also add the constraint that the total dose in each week should be equal to 95 and write it as

$$d_{ij} \geq 0, \qquad \sum_{j=1}^{5} d_{ij} = 95, \qquad i = 1, ..., 4. \tag{4.5}$$

Given a treatment schedule S, our constraint optimization problem is

$$\min_{D} C(t = 8.4) \tag{4.6}$$

with the constraint (4.5).

Example 2. *Consider a treatment schedule such that the virotherapy is applied on the Monday of week one with dose 95, and Thursday and Friday of week three, and Monday and Tuesday of week four, each with dose 47.5. The suitable values of each dose are obtained through the optimization simulation and, thus, the corresponding schedule and dosage matrices S and D are written as*

$$S = \begin{bmatrix} 1 & 0 & 0 & 0 & 0 \\ 0 & 0 & 0 & 0 & 0 \\ 0 & 0 & 0 & 1 & 1 \\ 1 & 1 & 0 & 0 & 0 \end{bmatrix}, \quad D = \begin{bmatrix} 95 & 0 & 0 & 0 & 0 \\ 0 & 0 & 0 & 0 & 0 \\ 0 & 0 & 0 & 47.5 & 47.5 \\ 47.5 & 47.5 & 0 & 0 & 0 \end{bmatrix}. \tag{4.7}$$

The optimization problem (4.6, 4.5) was solved numerically using MATLAB's `fmincon` routine (interior-point algorithm), which performs a gradient-based constrained nonlinear optimization. The system of ordinary differential equations (4.1) describing the oncolytic virus and immune–tumor dynamics was integrated at each iteration using `ode23s` with adaptive time stepping. The optimization was initialized using uniform or clinically motivated dose distributions and iterated until convergence criteria were satisfied (relative improvement in objective value $< 10^{-6}$).

In the first case in Figure 3, we distribute the initial viral dose of 95 over the first week of therapy. The cancer cell count remains low for some time period during the first week, which is slightly longer than the case of treatment on day 1 (Figure 2 top). While this schedule shows partial improvement, the cancer is not fully eradicated, and as a result, the TCP value remains at zero throughout the entire period. Next, in the middle row of Figure 3, we consider treatments in week one and two. A total dose of 190 is administered over two weeks, with four doses in total (95 per week). After the fourth dose on day 8, the cancer curve remains at zero for almost 30 days and the TCP shows a signal, a clear improvement compared to Figure 2 top.

To further investigate the effects of prolonged treatment, we distribute a total of 285 doses over three weeks in Figure 3 and over four weeks in Figure 4. In the three-week case, we see a clear treatment

success after day 15, where the TCP raises to 1. In the four-week treatments, we see good outcomes after 22 days.

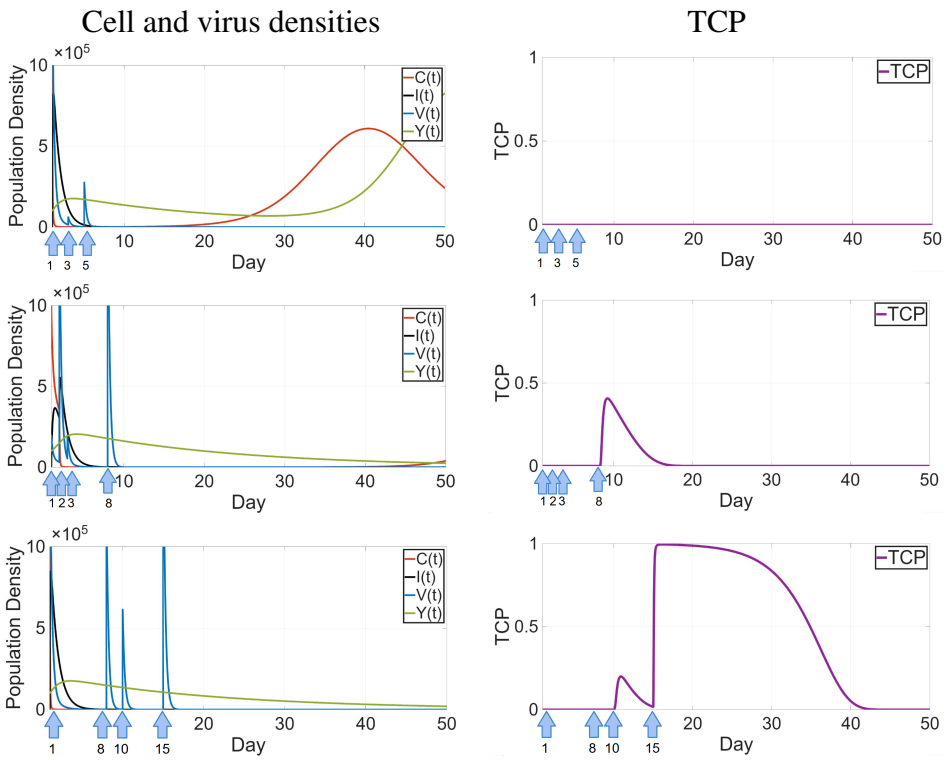

Figure 3. Strategy (S2), optimized scheduling. Examples of some of the optimized treatments. Left shows the dynamics of the cancer cells, virus, and immune cells and right the corresponding TCP. The density of virus particles are re-scaled by dividing by 100. The first row shows treatments on days 1 (with dose 78.94), 3 (2.33), and 5 (13.73), the second row on days 1 (10), 2 (77.76), 3 (7.24), and 8 (95), and third row days 1 (95), 8 (64.35), 10 (30.65), 15 (95). Note that we solve (2.2) numerically and rescale the results into dimensional variables such that we present densities and time in their physical units.

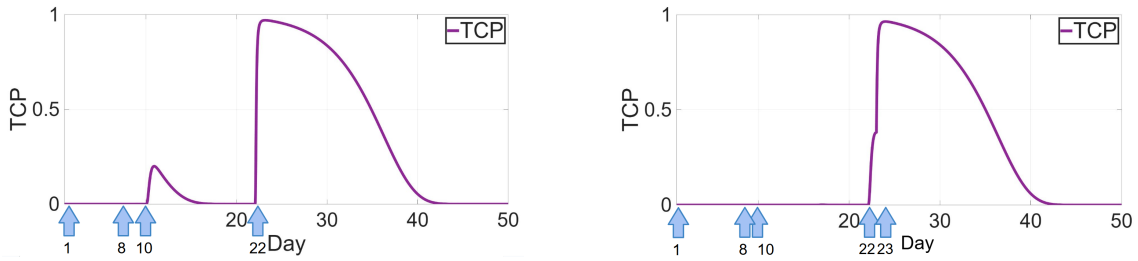

(a) **(b)**

Figure 4. Strategy (S2), optimized scheduling. (a): The TCP curve of 4 doses of virus of value of 285 on days 1 (value 95), day 8 (value 64.86), day 10 (value 3.14), and day 22 (value 95). (b): The TCP curve of 5 doses of virus of value of 285 on days 1 (value 95), day 15 (value 47.50), day 16 (value 47.50), day 22 (value 47.47), and day 23 (value 47.53).

We optimize many more schedules and we find a large number of successful schedules. We summarize them as a heat map in Figure 5. Each line in Figure 5 presents a schedule, where the days per week are the columns. On a treatment day, we use a color from dark red for a low dose to yellow for a high dose. The last column indicates the resulting maximum TCP. Bright yellow indicates successful cases. This figure illustrates the impact of various dosing schedules on the tumor control probability, highlighting how prolonged and optimized administration influences treatment outcomes. This aligns with the findings of Naumenko et al. [27], who suggested that while subsequent treatments may not have a direct infection effect, they enhance and sustain the infection initiated by the first viral dose, promote immune cell recruitment, and delay tumor growth.

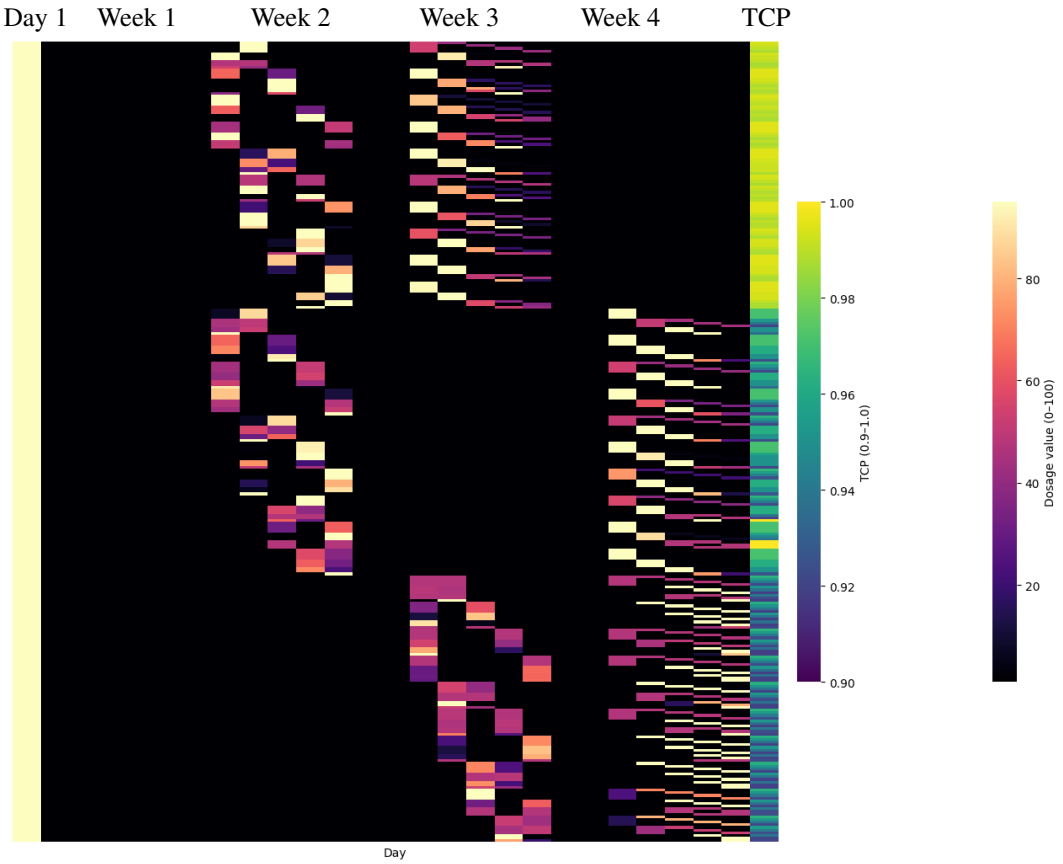

Figure 5. Summary of treatment schedules alongside their corresponding optimized dose values and the highest TCP values over a four-week period. Each row represents a schedule, where the days per week are the columns. On a treatment day we use a color from dark red for a low dose to yellow for a high dose. The last column indicates the resulting maximum TCP. We find a large set of good treatments, showing that scheduling matters and that several good strategies can be explored.

4.3. Strategies (S3): Combination of virotherapy and immunotherapies

As a result of tumor cell infection with OVs, an antitumor immune response is activated, transforming immunologically "cold" tumors into "hot" ones [30]. The lysis of tumor cells induced by OVs releases tumor antigens and stimulates the immune system, triggering immunogenic cell death. This

process leads to the release of danger-associated molecular patterns (DAMPs), pathogen-associated molecular patterns (PAMPs), and innate immune signaling molecules such as high mobility group box 1 (HMGB1) and adenosine diphosphate (ADP). Consequently, the immunosuppressive tumor microenvironment (TME) shifts to a proinflammatory state, activating innate immunity in nearby cells [31]. A combination of OVT and immuno therapies opens new avenues for developing more effective treatment regimens [32]. In this section, we will examine the efficacy of combining OVT with immune suppression, immune stimulation and with CAR-T cell therapy.

4.3.1. Strategy (S3a): Immunosuppression

The activation of the immune system may significantly limit viral replication and spread. This ultimately causes the reduction of the therapeutic efficacy of OVs [33]. The use of immunosuppressive drugs could be a strategy to inhibit this effect, as demonstrated in glioblastoma models, where systemic high-dose dexamethasone treatment or cyclophosphamide administration modulated and enhanced the efficacy of oncolytic virotherapy [34,35]. There has also been studies, which have shown that immunosuppressive treatment at the time of OVT did confer a negative impact on cancer survival and there was a trend toward worse overall survival, although not statistically significant [36]. In our model (2.2), we applied the immunosuppressive effect of the drugs with the factor ϵ_t. Our modified model is given as follows:

$$\begin{aligned} \frac{dC}{dt} &= C(1-C-I) - CV - pYC, \\ \frac{dI}{dt} &= CV - aI - qYI, \\ \frac{dV}{dt} &= \theta I - \gamma V - sVY, \\ \frac{dY}{dt} &= \epsilon_t \eta YC + \epsilon_t \zeta YI - \xi Y. \end{aligned} \tag{4.8}$$

We consider the effect of the drug only on the stimulation terms and not on the clearance rate. We study the results of the immunosuppression treatment combined with oncolytic virotherapy for different values of ϵ_t in Figure 6, and we do not observe any improvement in the TCP values of the system. We observe that the TCP values stayed zero (plots not shown), and thus the combination of these two treatments is one of the strategies that would not improve the outcome of OVT, according to our model.

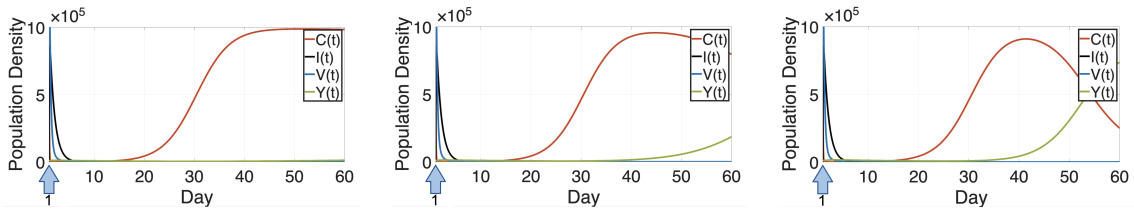

$\epsilon_t = 0.25$ $\epsilon_t = 0.50$ $\epsilon_t = 0.75$

Figure 6. Strategy (S3a) Immunosuppression: Dynamics of the infected and uninfected cancer cells, the virus, and the immune cells of model (4.8) in combination therapy of immunosuppressive drugs and oncolytic virotherapy for different values of ϵ_t. Again, the solutions are presented in dimensional coordinates. All the parameters are taken from Table 3.

We observe that immune suppression has almost no direct effect on the viral decline, indicating that viral clearance is primarily governed by other mechanisms. However, it exerts a pronounced impact on tumor control, as reducing the immune response allows cancer cells to proliferate more freely. This highlights the dual role of the immune system in OVT dynamics: while it can limit viral propagation by clearing infected cells and free virions, it is also essential for achieving effective tumor eradication. When immune activity is suppressed, the weakened antitumor response enables tumor regrowth despite the presence of the virus, underscoring the importance of maintaining a balanced immune function during virotherapy.

4.3.2. Strategy (S3b): Immune stimulation

One of the promising strategies of OVs enhancement is to combine them with the use of T-cell engager molecules. This stimulates existing T cells to lyse tumor cells [4]. Scientists might call the immune modulators as the gas pedals of the immune system. Different types of therapies have been developed that improve the immune system's ability to attack and eliminate cancer [37]. Similarly, we add the factor χ of immune stimulator to the model (2.2). The model is given in Eq (4.9).

$$\begin{aligned} \frac{dC}{dt} &= C(1-C-I) - CV - \chi pYC, \\ \frac{dI}{dt} &= CV - aI - \chi qYI, \\ \frac{dV}{dt} &= \theta I - \gamma V - \chi sVY, \\ \frac{dY}{dt} &= \chi\eta YC + \chi\zeta I - \xi Y. \end{aligned} \tag{4.9}$$

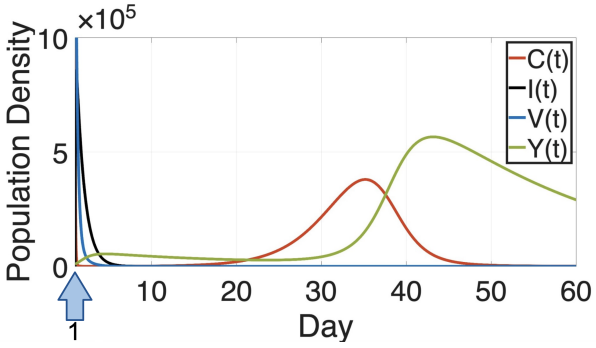

Figure 7. Strategy (S3b) immune stimulation: Dynamics of the infected and uninfected cancer cells, the virus, and the immune cells in combination therapy of immunostimulation drugs modulating the immune system by a factor of $\chi = 2.5$ and oncolytic virotherapy for model (4.9).

The results we obtained showed no improvement in the outcome of the treatment. In Figure 7, after modulating the immune system by a factor of 2.5, we observe that it temporarily reduces the tumor load in an oscillatory manner; however, the TCP plot remains sustained at zero (plots not shown). In our baseline case, the virus is already relatively weak and unable to achieve tumor eradication on its own. Enhancing the immune response further lowers viral replication and spread, thereby reducing the

therapeutic potential of the virus. As a result, a moderate increase in immune activity does not lead to a favorable balance between viral replication and immune clearance. In this setting, immune stimulation contributes primarily through direct antitumor effects rather than by supporting the virotherapy, effectively shifting the mechanism toward pure immunotherapy rather than combined oncolytic treatment.

4.3.3. Strategy (S3c): Combination with CAR-T cells therapy

Our next strategy for improving the OVT efficacy is its combination with CAR-T cell therapy. In this therapy, in order to help T-cells recognize tumor-derived antigens, T-cells are extracted from the patient's body, genetically engineered to express CARs, and then they are infused back to the patient [38]. However, it has been shown that tumor-mediated immunosuppression is one of the biggest challenges in CAR-T cell therapy [39]. By combining OVT and CAR-T cell therapy, oncolytic viruses infect the tumor cells and make infected cells express target tumor antigens that are recognized by CAR-T cells [40].

Figure 8 helps to have a better understanding of how the infected, uninfected cancer cells interact with the virus and the CAR-T cells.

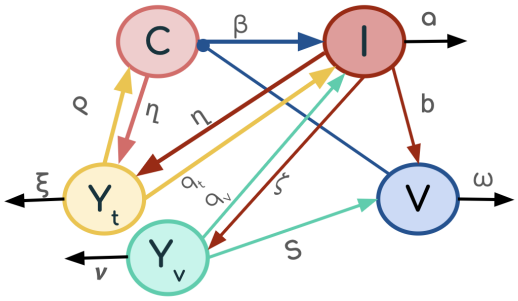

Figure 8. Sketch of the OVT-CAR-T model. The blue arrows represent the viral infection of cancer cells at a rate of β. The red arrow shows the burst of viruses released from lysed infected cells at rate b. The light cyan arrows indicate the virus-induced cancer cell killing of the T cells at rate σ, while the orange arrows illustrates their direct killing of the virus and the cancer cells at rates λ and δ_T, respectively. The pink and red arrows denote denote the CAR-T cell death by the cancer cells at rate μ. All black arrows depict cell death and virus degradation.

Our base CAR-T cell ODE model in dimensional form is as follows:

$$\begin{aligned}
\frac{dC}{dt} &= rC\left(1-\frac{C+I}{L}\right)-\beta CV-\delta_T CT-\sigma VCT,\\
\frac{dI}{dt} &= \beta CV-\alpha I-\delta_T IT-\sigma VIT,\\
\frac{dV}{dt} &= \alpha bI-\omega V-\lambda VT+\tilde{u}(t),\\
\frac{dT}{dt} &= \rho\,(C+I)\,T+\kappa TV-\mu(C+I)T-\upsilon T.
\end{aligned} \tag{4.10}$$

In this model, similar to our base model (2.1), we consider C and I to represent the populations of

uninfected and infected cancer cells, respectively. We introduce T as both the CAR-T cell population and the general immune cells that targets both cancer cells and free viruses— noting that effector CAR-T cells alone only target cancer cells. Additionally, the population of free viruses (V) is represented in the third equation. The first two terms in equation one are similar as in model (2.1). The third and forth terms account for tumor cell killing by the effector CAR-T cells at rates δ_T and σ respectively, but the difference is that the fourth term denotes the OV-induced CAR-T killing. Terms one and two in the infected cancer cells equation are the same as in Eq (2.1), and the two following terms represent the CAR-T cell killing similar to the first equation. In equation three, we have the effective replication term of the virus and their clearance in terms one and two respectively, and the last term denotes the killing of the OV by the immune cells. $\tilde{u}(t)$ is the dimensional control term and has a similar definition as (4.4) after non-dimensionalization. ρ represents the rate at which CAR-T/immune cells are stimulated and proliferate upon interacting with both infected and uninfected cancer cells, as described in the first term of equation four. The second term represents an OV-induced recruitment of CAR-T cells at rate κ inspired from [41]. The third term denotes the inactivation of CAR-T cells by both types of the tumor cells at the rate μ and their natural death at rate υ is accounted for in the last term.

In this model, the similar parameters as the Eq (2.1) have the same values as in Table 2. The rest of the parameter values are given in Table 4.

Table 4. Model parameters for the onco-virus CAR-T cell model (4.10), and their baseline values, units, and references. Parameters not listed here are given in Table 2.

Parameter	Description	Baseline value	Units	Source
δ_T	Killing rate of tumor cells by CAR-T cells	10^{-7} $(3.7\times10^{-6}, 3.36\times10^{-8})$	$(\text{cell}\cdot\text{day})^{-1}$	[38,41]
σ	Tumor cell proliferation rate	0.23×10^{-9}	$(\text{virus}\cdot\text{cell}\cdot\text{day})^{-1}$	[41] (estimated)
λ	Killing rate of virus by immune cells	0.21×10^{-6}	$(\text{cell}\cdot\text{day})^{-1}$	[10] (estimated)
ρ	CAR-T cells proliferation rate	6×10^{-6} $(2.3\times10^{-6}, 6\times10^{-6})$	$(\text{cell}\cdot\text{day})^{-1}$	[38]
κ	Virus-induced CAR-T cell recruitment rate	1.5×10^{-10}	$(\text{virus}\cdot\text{day})^{-1}$	(estimated)
μ	Immune cell exhaustion rate	4.5×10^{-8}	$(\text{cell}\cdot\text{day})^{-1}$	[38]
υ	Natural death rate of immune cells	0.350	$(\text{day})^{-1}$	[38]

The parameters that are taken from Mahasa et al. [41] are from their study of glioma and the hrR3 virus. The CAR-T cell parameters from Barros et al. [38] are taken from their study on CAR-T cell therapy for mice with Hodgkin's disease.

We set the initial conditions to be

$$C(0) = 10^6, \quad I(0) = 0, \quad V(0) = 1.9\times10^{10}, \quad T(0) = 2\times10^5. \tag{4.11}$$

In Figure 9, we show several cases of treatment timing. In the first row of Figure 9, we first simulate the behavior of model (4.10) after non-dimenstionalization in the absence of virotherapy ($\frac{dV}{dt} = 0, V_0 = 0$).

We start the simulations without considering any optimization, and thus, the control term $\tilde{u}(t)$ in (4.10) is zero. In Figure 9(a), we see that although this monotherapy brings the cancer cells significantly down for a long time, the TCP curve only rises to slightly over 0.6. Combination of these two therapies is one of the suggested strategies to improve the efficacy of the treatments [42–44]. As OVs are armed with therapeutic transgenes, this causes a boost in the CAR-T activation. Also, in the immunosuppressed tumor's microenvironment, OVs could be able to survive and even maintain their

cytotoxicity functions [42]. When combined, we see in Figure 9(b) that the TCP value has a quick jump to about 0.98 just by an injection of CAR-T cells and the OV on day one. This shows the importance of the combination of virotherapy with immunotherapy for treatment efficacy and patients benefit.

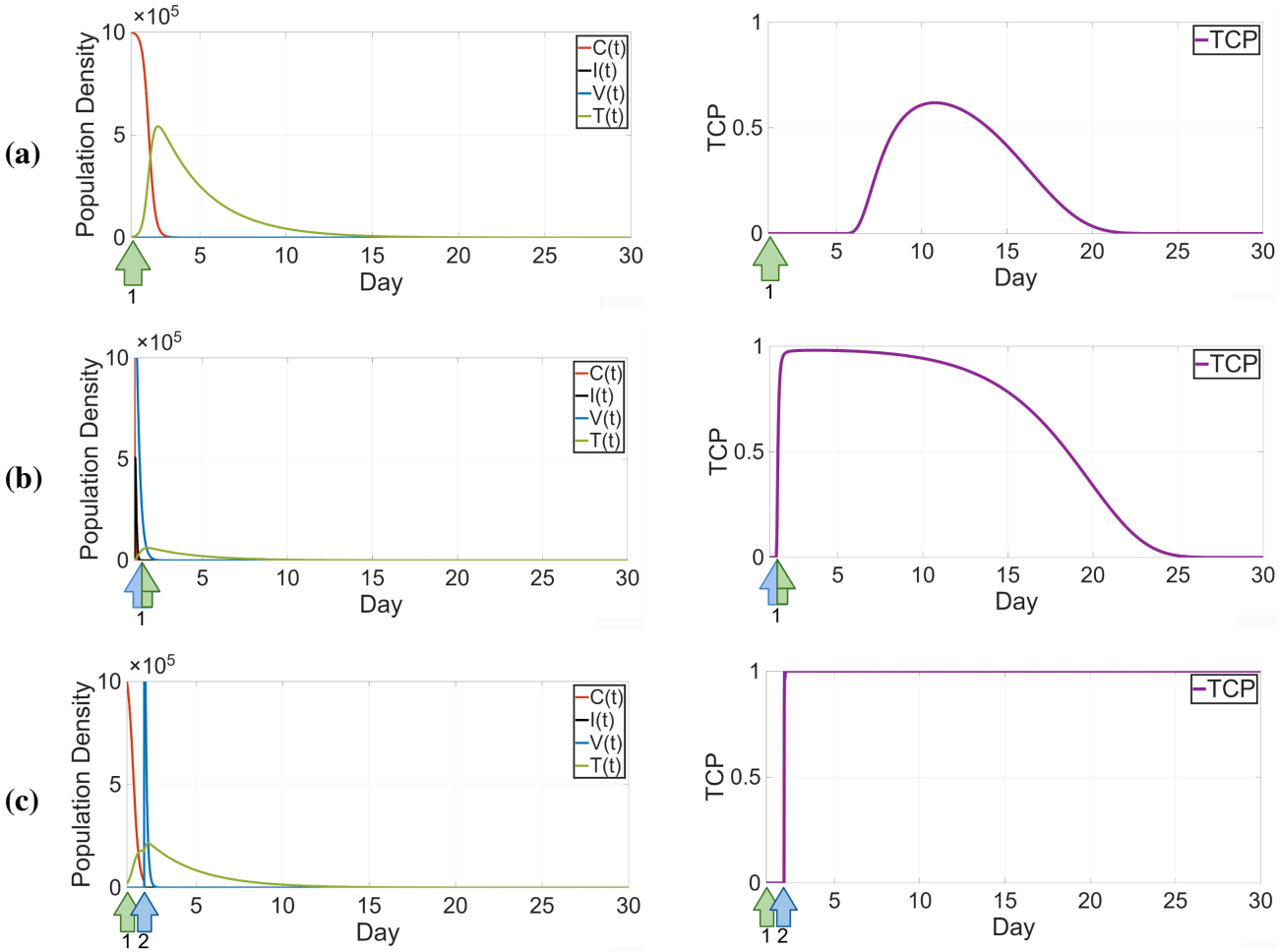

Figure 9. Strategy (S3c) combined with CAR-T: Dynamics of cancer cells and CAR-T cells in model (4.10) and the corresponding TCP. The density of virus particles are re-scaled by dividing by 10^4 and CAR-T cells by 100. **(a)** A single dose of CAR-T cells without oncolytic virus. **(b)** CAR-T cells and oncolytic virus both administered on day one. **(c)** Optimized treatment: CAR-T therapy on day one and virus injection on day two.

We apply a similar optimizing strategy as in model (4.1) by considering similar restrictions for the combination of CAR-T cells and virotherapy model (4.10) after non-dimensionalization. The goal is to improve the results we obtained from the non-optimized combination therapy.

We test different schedules to obtain a more optimal boost for this combination therapy. During optimization simulations, we observe that by a slight delay in the administration of the initial virus dose, a more minimized tumor load is achieved as this delay significantly improved treatment outcomes. As we see in Figure 9 row (c), when CAR-T cell therapy is administered on day one, followed by oncolytic virus treatment on day two, the outcome is significantly more effective. The initial CAR-T cell injection reduces the cancer cell population. Once the tumor burden is lowered, virotherapy starts. At

this stage, in addition to directly infecting cancer cells, OVs act as a booster for CAR-T cells as well. When the delay between the OVT and CAR-T cell administration is increased, the treatment remains effective; however, excessively long delays allow the tumor to repopulate, which can reduce the overall probability of tumor eradication. Therefore, while introducing a delay between therapies can be beneficial, its duration must be carefully optimized. An appropriately timed delay can enhance treatment synergy and maximize TCP, whereas an overly long interval may compromise therapeutic success.

4.4. Sensitivity analysis of treatment parameters

To evaluate the robustness of the proposed treatment protocols, we performed a sensitivity analysis of the TCP with respect to key biological parameters. Starting from the baseline TCP shown in Figure 9(a), we systematically varied selected parameters within physiologically relevant ranges and plotted the resulting TCP bands (Figure 10).

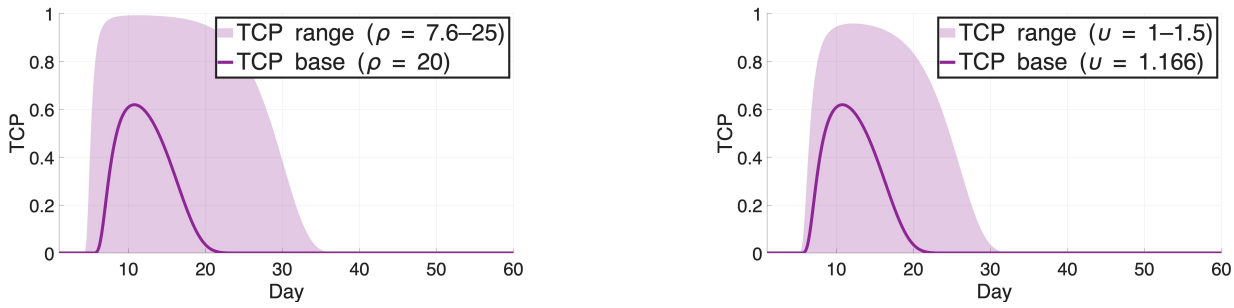

Figure 10. TCP for CAR-T cell therapy alone. The figure on the left shows the sensitivity to the CAR-T stimulation by cancer cells parameter (ρ), while the figure on the right shows the sensitivity to the CAR-T cell clearance parameter (υ). All other parameters are at base value in Table 4.

For the CAR-T–only treatment, the TCP was moderately sensitive to the proliferation rate parameter ρ and the CAR-T clearance rate υ. The TCP increased substantially when ρ approached higher values (around 2) or when υ decreased from its baseline value of 1.1 to 1, suggesting that slower CAR-T clearance enhances therapeutic performance.

In contrast, when OVT and CAR-T treatments were applied simultaneously (Figure 11), the TCP curve remained relatively stable, showing reduced sensitivity to parameter variations. The combined therapy maintained a high TCP across the entire range of parameter perturbations.

Finally, when a 1–4 days delay between OVT and CAR-T administrations was introduced, the TCP remained close to 1 even under significant parameter variations. This observation indicates that the delayed combination protocol is robust and capable of achieving successful tumor control across a broad spectrum of biological conditions.

We summarize the outcome of our various strategies in Table 5. Successful treatments are shown in bold.

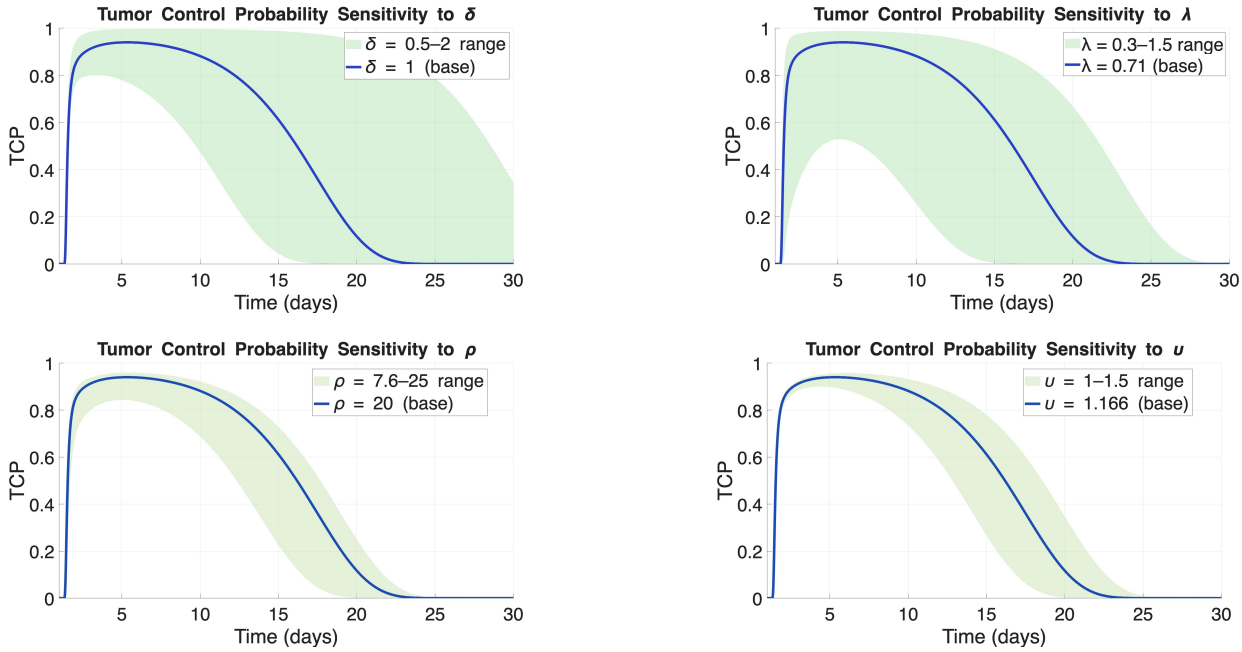

Figure 11. TCP for simultaneous CAR-T cell and OVT on day one. The shaded region indicates the sensitivity of the TCP curve to variations in the corresponding parameter within the specified range. The figure on the top left shows the sensitivity to the CAR-T cell killing of infected and uninfected cancer cells (δ); the top right shows the sensitivity to viral clearance by CAR-T cells (λ). The bottom left panel shows the sensitivity to the CAR-T stimulation by cancer cells parameter (ρ), and the bottom right panel shows the sensitivity to the CAR-T cell clearance parameter (υ). All other parameters are at base value in Table 4.

5. Conclusions

Using a virus to treat cancer is an intriguing idea. Research on oncolytic viruses is at full swing and some have made it already through clinical trials and FDA approvals [45]. However, the efficacy of OV therapy, even for approved viruses, is rather limited because of physical barriers, tumor heterogeneity, and an immunosuppressive tumor microenvironment [46]. Several strategies to improve the efficacy of OV therapy are currently considered. Researchers genetically modify viruses to make them stronger, more or less infective, diffuse faster, and reproduce better [47]. The combination of OV with different methods of immunotherapy has been extensively studied because OV is a natural activator of both innate and adaptive immunity [48]. However, treatment scheduling as an approach to increase the efficacy of OV therapy, has so far been ignored. Here, we use a mathematical model to compare OVT and OVT combination therapies with optimized treatment scheduling.

Our analysis confirmed earlier findings that OVT, when used as a monotherapy at baseline values, is insufficient to fully eradicate cancer cells or prevent tumor relapse following treatment. To enhance the therapeutic outcome of OVT, we explored several strategies. We first examined the effect of increasing the effective viral production rate. Although this demonstrated a significant improvement in therapeutic outcomes, achieving such levels remains unrealistic with the viral strains currently existing in clinical use. A particularly novel contribution of this study was the implementation of optimized

dosing and scheduling of OVT within our model. Simulation results highlighted the critical importance of secondary dosing. In fact we found a large set of effective treatment schedules (see Figure 5), each involving OV treatments that could even be two weeks apart from each other.

Notably, the therapeutic benefit of OVT following the initial dose was not primarily due to direct infection of target cells, but rather its role in stimulating and boosting the immune response. Our final strategy involved combining OVT with immunotherapies. The first combination tested included immunosuppression and immune stimulation. Neither approach enhanced the effectiveness of OVT: in the case of immunosuppression, OVT remained too weak to eradicate the infection on its own; in contrast, immune stimulation alone cleared the virus more aggressively, undermining the potential benefits of OV therapy. Our final combination therapy was the combination of OVT with CAR-T cell therapy. Using our optimization framework, we found that the most effective treatment outcome occurred when OVT was applied a day after immune therapy was administered. This was because simultaneous application hindered proper stimulation of CAR-T cells by initial rapid reduction of cancer cells. A summary of these results is given in Table 5.

Table 5. Summary of treatment strategies, schedules, viral doses, and TCP for model (2.1). The most promising combinations are shown in bold.

Strategy	Treatment week (s)	Schedule (Days)	Total Dose	Max TCP	Normalized AUC
(S1) Increasing θ	Week 1	Day 1 (θ = 58)	95	0	0
	Week 1	Day 1 (θ = 350)	95	0.39	0.029
	Week 1	**Day 1 (θ = 500)**	**95**	**0.96**	**0.217**
(S2) Optimized schedule	Week 1	Days 1, 3	95	0	0
	Weeks 1, 2	Days 1, 2, 3, 8	190	0.40	0.025
	Weeks 1, 2, 3	**Days 1, 8, 10, 15**	**285**	**0.99**	**0.397**
	Weeks 1, 2, 4	**Days 1, 15, 16, 22, 23**	**285**	**0.97**	**0.254**
	Weeks 1, 3, 4	**Days 1, 8, 9, 22**	**285**	**0.96**	**0.246**
		Combination therapies			
(S3a) Immunosuppression (ϵ_t)	Week 1	Day 1 (ϵ_t = 0.25)	95	0	0
	Week 1	Day 1 (ϵ_t = 0.5)	95	0	0
	Week 1	Day 1 (ϵ_t = 0.75)	95	0	0
(S3b) Immunostimulation (χ = 2.5)	Week 1	Day 1	95	0	0
(S3c) CAR-T Model (A)	Week 1	CAR-T: Day 1	CAR-T: 2	0.62	0.09
	Week 1	CAR-T: Day 1, OV: Day 1	CAR-T: 2, OV: 95	0.98	0.275
	Week 1	**CAR-T: Day 1, OV: Day 2**	**CAR-T: 2, OV: 95**	**1**	**0.963**
(S3c) CAR-T Model (B)	Week 1	CAR-T: Day 1	CAR-T: 2	0.6	0.0875
	Week 1	CAR-T: Day 1, OV: Day 1	CAR-T: 2, OV: 95	0	0
	Week 1	**CAR-T: Day 1, OV: Day 2**	**CAR-T: 2, OV: 95**	**1**	**0.979**

The model that we use here is not calibrated to a single tumor or a single virus type. Hence, the optimized treatments identified here are not applicable to patients. However, we show that much can be gained by varying OVT scheduling, and it is worthwhile to further explore treatment scheduling in more detail for specific cancers and specific viruses.

In the models presented in this work, immune effects were represented through a single global immune compartment that encompassed immune cells responding to cancer cells, viral antigens, and CAR-T cells. However, immune interactions are inherently more specific, and we also considered a version of the model where we distinguish between immune responses according to their specific targets—cancer cells, viral antigens, and CAR-T cells (see Appendix B). In Section B.1, we introduce

a model that separates CAR-T cells from the general immune population, and in Section B.2, we extend the framework further to include distinct immune compartments targeting the virus and cancer cells, respectively. Our findings of such an extended models are consistent with the earlier results, namely, that an appropriate choice of viral treatment schedule has a substantial impact on therapeutic outcomes.

The cancer, the virus, and the immune response live in a spatial domain, and spatial effects might be important, too. In [9] and [49], the base model for oncolytic virus therapy including diffusion terms was studied. It describes the interactions between uninfected cancer cells, infected cancer cells, and free virus particles within a spatial domain Ω and is given by the following system of partial differential equations:

$$\begin{aligned} \frac{\partial C}{\partial t} &= D_C \Delta C + rC\left(1 - \frac{C+I}{L}\right) - \beta CV, \\ \frac{\partial I}{\partial t} &= D_I \Delta I + \beta CV - \alpha I, \\ \frac{\partial V}{\partial t} &= D_V \Delta V + \alpha b I - \omega V, \end{aligned} \tag{5.1}$$

with homogeneous Neumann boundary conditions on $\partial\Omega$. The above PDE describes a system of spatially coupled oscillators, and the authors in [9] found that spatially complex patterns can arise, including hollow-ring patterns, traveling waves, and spiral waves. In [49] it was further shown that the above PDE can be transformed into a $\lambda - \omega$ model, which is a normal form for spiral waves [50]. This shows that spatial communtication between cells and viruses can lead to largely heterogeneous effects, and the significance of these effects for OVT still needs to be explored.

Use of AI tools declaration

The authors declare they have not used Artificial Intelligence (AI) tools in the creation of this article.

Acknowledgments

We are particularly grateful to discussions with Morgan van Walsum during her NSERC-USRA 2024 scholarship at the University of Alberta. We also thank the Math Bio Journal Club for helpful comments. NM acknowledges the funding support from the University of Alberta. TH is supported through a discovery grant of the Natural Science and Engineering Research Council of Canada (NSERC), RGPIN-2023-04269.

Conflict of interest

The authors declare there is no conflict of interest.

References

1. C. E. Engeland, J. C. Bell, Introduction to oncolytic virotherapy, in *Oncolytic Viruses* (Ed. C. E. Engeland), Springer, New York, NY, (2020), 1–6. https://doi.org/10.1007/978-1-4939-9794-7_1

2. D. Lin, Y. Shen, T. Liang, Oncolytic virotherapy: Basic principles, recent advances and future directions, *Signal Transduction Targeted Ther.*, **8** (2023), 156. https://doi.org/10.1038/s41392-023-01407-6

3. F. Maryam, S. Gul, Mechanisms, challenges and future prospects of oncolytic virotherapy: A comprehensive review, *J. Curr. Oncol. Med. Sci.*, **4** (2024), 813–827.

4. G. Marelli, A. Howells, N. R. Lemoine, Y. Wang, Oncolytic viral therapy and the immune system: A double-edged sword against cancer, *Front. Immunol.*, **9** (2018), 866. https://doi.org/10.3389/fimmu.2018.00

5. N. Mohammadnejad, T. Hillen, Stacked waves and qualitative analysis of an oncolytic virus–immune model, *bioRxiv*, 2025. submitted for publication. https://doi.org/10.1101/2025.09.04.674336

6. Y. Kim, D. R. Clements, A. M. Sterea, H. W. Jang, S. A. Gujar, P. W. K. Lee, Dendritic cells in oncolytic virus-based anti-cancer therapy, *Viruses*, **7** (2015), 6506–6525. https://doi.org/10.3390/v7122953

7. M. Jafari, M. Kadkhodazadeh, M. B. Shapourabadi, N. H. Goradel, M. A. Shokrgozar, A. Arashkia, et al., Immunovirotherapy: The role of antibody-based therapeutics in combination with oncolytic viruses, *Front. Immunol.*, **13** (2022), 1012806. https://doi.org/10.3389/fimmu.2022.1012806

8. R. L. Martuza, A. Malick, J. M. Markert, K. L. Ruffner, D. M. Coen, Experimental therapy of human glioma by means of a genetically engineered virus mutant, *Science*, **252** (1991), 854–856. https://doi.org/10.1126/science.1851332

9. A. A. Baabdulla, T. Hillen, Oscillations in a spatial oncolytic virus model, *Bull. Math. Biol.*, **86** (2024), 93. https://doi.org/10.1007/s11538-024-01322-z

10. S. M. Al-Tuwairqi, N. O. Al-Johani, E. A. Simbawa, Modeling dynamics of cancer virotherapy with immune response, *Adv. Differ. Equations*, **2020** (2020), 438. https://doi.org/10.1186/s13662-020-02893-6

11. D. Wodarz, Viruses as antitumor weapons: Defining conditions for tumor remission, *Cancer Res.*, **61** (2001), 3501–3507.

12. D. Wodarz, N. Komarova, Towards predictive computational models of oncolytic virus therapy: Basis for experimental validation and model selection, *PLoS One*, **4** (2009), e4271. https://doi.org/10.1371/journal.pone.0004271

13. N. L. Komarova, D. Wodarz, ODE models for oncolytic virus dynamics, *J. Theor. Biol.*, **263** (2010), 530–543. https://doi.org/10.1016/j.jtbi.2010.01.009

14. J. P. Tian, The replicability of oncolytic virus: Defining conditions in tumor virotherapy, *Math. Biosci. Eng.*, **8** (2011), 841–860. https://doi.org/10.3934/mbe.2011.8.841

15. R. Eftimie, J. Dushoff, B. W. Bridle, J. L. Bramson, D. J. D. Earn, Multi-stability and multi-instability phenomena in a mathematical model of tumor–immune–virus interactions, *Bull. Math. Biol.*, **73** (2011), 2932–2961. https://doi.org/10.1007/s11538-011-9653-5

16. K. M. Storey, S. E. Lawler, T. L. Jackson, Modeling oncolytic viral therapy, immune checkpoint inhibition, and the complex dynamics of innate and adaptive immunity in glioblastoma treatment, *Front. Physiol.*, **11** (2020), 151. https://doi.org/10.3389/fphys.2020.00151

17. P. Pooladvand, C. O. Yun, A. R. Yoon, P. S. Kim, F. Frascoli, The role of viral infectivity in oncolytic virotherapy outcomes: A mathematical study, *Math. Biosci.*, **334** (2021), 108520. https://doi.org/10.1016/j.mbs.2020.108520

18. J. T. Wu, H. M. Byrne, D. H. Kirn, L. M. Wein, Modeling and analysis of a virus that replicates selectively in tumor cells, *Bull. Math. Biol.*, **63** (2001), 731–768. https://doi.org/10.1006/bulm.2001.0245

19. H. F. Lodish, *Molecular Cell Biology*, Macmillan, 2008.

20. J. H. Kim, Y. S. Lee, H. Kim, J. H. Huang, A. R. Yoon, C. O. Yun, Relaxin expression from tumor-targeting adenoviruses and its intratumoral spread, apoptosis induction, and efficacy, *JNCI J. Natl. Cancer Inst.*, **98** (2006), 1482–1493. https://doi.org/10.1093/jnci/djj397

21. A. Friedman, J. P. Tian, G. Fulci, E. A. Chiocca, J. Wang, Glioma virotherapy: Effects of innate immune suppression and increased viral replication capacity, *Cancer Res.*, **66** (2006), 2314–2319. https://doi.org/10.1158/0008-5472.CAN-05-2661

22. S. Gujar, J. G. Pol, G. Kroemer, Heating it up: Oncolytic viruses make tumors "hot" and suitable for checkpoint blockade immunotherapies, *OncoImmunology*, **7** (2018), e1442169. https://doi.org/10.1080/2162402X.2018.1442169

23. J. Gong, M. M. D. Santos, C. Finlay, T. Hillen, Are more complicated tumour control probability models better, *Math. Med. Biol.*, **30** (2013), 1–19. https://doi.org/10.1093/imammb/dqr023

24. R. D. Yates, *Probability and Stochastic Processes: A Friendly Introduction for Electrical and Computer Engineers*, John Wiley & Sons, Inc., 2014.

25. E. V. Shashkova, S. M. May, M. A. Barry, Characterization of human adenovirus serotypes 5, 6, 11, and 35 as anticancer agents, *Virology*, **394** (2009), 311–320. https://doi.org/10.1016/j.virol.2009.08.038

26. M. S. C. Ornella, J. J. Kim, E. Cho, M. Cho, T. H. Hwang, Dose considerations for vaccinia oncolytic virus based on retrospective reanalysis of early and late clinical trials, *Vaccines*, **12** (2024), 1010. https://doi.org/10.3390/vaccines12091010

27. V. Naumenko, J. Rajwani, M. Turk, C. Zhang, M. Tse, R. P. Davis, et al., Repeated dosing improves oncolytic rhabdovirus therapy in mice via interactions with intravascular monocytes, *Commun. Biol.*, **5** (2022), 1–14. https://doi.org/10.1038/s42003-022-04254-3

28. M. A. Currier, L. C. Adams, Y. Y. Mahller, T. P. Cripe, Widespread intratumoral virus distribution with fractionated injection enables local control of large human rhabdomyosarcoma xenografts by oncolytic herpes simplex viruses, *Cancer Gene Ther.*, **12** (2005), 407–416. https://doi.org/10.1038/sj.cgt.7700799

29. *International Virotherapy Center*, *RIGVIR® Guidelines on the Use in Oncology (Public Version for Informational Purposes)*, 2024. Available from: https://www.virotherapy.com/doc/IVC-Rigvir-Guidelines-in-Oncology_10.2024.pdf. [Accessed: 19 Oct 2025]

30. M. Garofalo, K. W. Pancer, M. Wieczorek, M. Staniszewska, M. Wieczorek, L. Kuryk, et al., From immunosuppression to immunomodulation – turning cold tumours into hot, *J. Cancer*, **13** (2022), 2884–2892. https://doi.org/10.7150/jca.71992

31. R. Burchett, S. Walsh, Y. Wan, J. L. Bramson, A rational relationship: Oncolytic virus vaccines as functional partners for adoptive T cell therapy, *Cytokine Growth Factor Rev.*, **56** (2020), 149–159. https://doi.org/10.1016/j.cytogfr.2020.07.003

32. A. Ageenko, N. Vasileva, V. Richter, E. Kuligina, Combination of oncolytic virotherapy with different antitumor approaches against glioblastoma, *Int. J. Mol. Sci.*, **25** (2024), 2042. https://doi.org/10.3390/ijms25042042

33. A. L. De Matos, L. S. Franco, G. McFadden, Oncolytic viruses and the immune system: The dynamic duo, *Mol. Ther. Methods Clin. Dev.*, **17** (2020), 349–358. https://doi.org/10.1016/j.omtm.2020.01.001

34. G. Fulci, L. Breymann, D. Gianni, K. Kurozomi, S. S. Rhee, J. Yu, et al., Cyclophosphamide enhances glioma virotherapy by inhibiting innate immune responses, *Proc. Natl. Acad. Sci. U.S.A.*, **103** (2006), 12873–12878. https://doi.org/10.1073/pnas.0605496103

35. M. S. Koch, M. Zdioruk, M. O. Nowicki, A. M. Griffith, E. Aguilar, L. K. Aguilar, et al., Systemic high-dose dexamethasone treatment may modulate the efficacy of intratumoral viral oncolytic immunotherapy in glioblastoma models, *J. Immunother. Cancer*, **10** (2022), e003368. https://doi.org/10.1136/jitc-2021-003368

36. A. Tison, G. Quéré, L. Misery, E. Funck-Brentano, F. X. Danlos, E. Routier, et al., Safety and efficacy of immune checkpoint inhibitors in patients with cancer and preexisting autoimmune disease: A nationwide, multicenter cohort study, *Arthritis Rheumatol.*, **71** (2019), 2100–2111. https://doi.org/10.1002/art.41068

37. *Cancer Research Institute*, *Immunomodulators: Checkpoint Inhibitors, Cytokines, Agonists, and Adjuvants*, Available from: https://www.cancerresearch.org/treatment-types/immunomodulators. [Accessed: 14-Feb-2025]

38. L. R. C. Barros, E. A. Paixão, A. M. P. Valli, G. T. Naozuka, A. C. Fassoni, R. C. Almeida, CART math: A mathematical model of CAR-T immunotherapy in preclinical studies of hematological cancers, *Cancers*, **13** (2021), 2934. https://doi.org/10.3390/cancers13122934

39. S. Zuo, M. Wei, B. He, A. Chen, S. Wang, L. Kong, et al., Enhanced antitumor efficacy of a novel oncolytic vaccinia virus encoding a fully monoclonal antibody against T-cell immunoglobulin and ITIM domain (TIGIT), *EBioMedicine*, **64** (2021), 103240. https://doi.org/10.1016/j.ebiom.2021.103240

40. G. V. Kochneva, G. F. Sivolobova, A. V. Tkacheva, A. A. Gorchakov, S. V. Kulemzin, Combination of oncolytic virotherapy and CAR T/NK cell therapy for the treatment of cancer, *Mol. Biol.*, **54** (2020), 1–12. https://doi.org/10.1134/S0026893320010100

41. K. J. Mahasa, R. Ouifki, A. Eladdadi, L. de Pillis, A combination therapy of oncolytic viruses and chimeric antigen receptor T cells: A mathematical model proof-of-concept, *Math. Biosci. Eng.*, **19** (2022), 4429–4457. https://doi.org/10.3934/mbe.2022205

42. E. Ponterio, T. L. Haas, R. De Maria, Oncolytic virus and CAR-T cell therapy in solid tumors, *Front. Immunol.*, **15** (2024), 1455163. https://doi.org/10.3389/fimmu.2024.1455163

43. M. Conte, A. Xella, R. T. Woodall, K. A. Cassady, S. Branciamore, C. E. Brown, et al., CAR T-cell and oncolytic virus dynamics and determinants of combination therapy success for glioblastoma, Cold Spring Harbor Laboratory Press, United States, *bioRxiv*, 2025.
44. J. He, F. Munir, D. Ragoonanan, W. Zaky, S. J. Khazal, P. Tewari, et al., Combining CAR T cell therapy and oncolytic virotherapy for pediatric solid tumors: A promising option, *Immuno*, **3** (2023), 37–56. https://doi.org/10.3390/immuno3010004
45. S. L. Greig, Talimogene laherparepvec: First global approval, *Drugs*, **76** (2016), 147–154. https://doi.org/10.1007/s40265-015-0522-7
46. S. J. Russell, G. N. Barber, Oncolytic viruses as antigen-agnostic cancer vaccines, *Cancer Cell*, **33** (2018), 599–605.
47. A. A. Baabdulla, F. Cristi, M. Shmulevitz, T. Hillen, Mathematical modelling of reoviruses in cancer cell cultures, *PLoS One*, **20** (2025), e0318078. https://doi.org/10.1371/journal.pone.0318078
48. C. M. Oh, H. J. Chon, C. Kim, Combination immunotherapy using oncolytic virus for the treatment of advanced solid tumors, *Int. J. Mol. Sci.*, **21** (2020), 7743. https://doi.org/10.3390/ijms21207743
49. T. Bansod, *Spiral Waves in Oncolytic Virotherapy and Patch Formation in Gene Networks*, Master's Thesis, University of Alberta, 2025.
50. J. D. Murray, *Mathematical Biology*, Biomathematics, Springer, **19** (1989). https://doi.org/10.1007/978-3-662-08539-4
51. K. J. Mahasa, A. Eladdadi, L. De Pillis, R. Ouifki, Oncolytic potency and reduced virus tumor-specificity in oncolytic virotherapy: A mathematical modelling approach, *PLoS One*, **12** (2017), e0184347. https://doi.org/10.1371/journal.pone.0184347
52. R. R. Rich, T. A. Fleisher, W. T. Shearer, H. W. Schroeder Jr, C. M. Weyand, D. B. Corry, et al., *Clinical Immunology: Principles and Practice*, 6th edition, Elsevier, 2022.

Appendix

A. Parameter values from the literature

Table A1 summarizes and compares the key model parameters used in different oncolytic virotherapy modeling studies. The values illustrate the variability in parameter choices across the literature, reflecting differences in biological assumptions, tumor types, and model formulations. Our parameter set is included for reference and consistency within the present work.

Table A1. Comparison of parameters used across different studies.

Parameter used in paper	r	β	α	b	γ
Units	day^{-1}	$(\text{virus}\cdot\text{day})^{-1}$	day^{-1}	$(\text{virus})(\text{cell})^{-1}$	day^{-1}
Baadbullah et al. [9]	0.3	1.5×10^{-9}	1	58.33	4
Al Tuwairqi [10]	0.48	16.8×10^{-9}	1.33	50	0.28
Mahasa et al. [51]	0.072	1.7×10^{-8}	1	1350	0.6
Friedman et al. [21]	0.48	16.8×10^{-9}	1.33	50	0.6
Our parameters	0.3	1.5×10^{-9}	1	58.33	4

B. Modeling with separate immune compartments

B.1. Separate compartments for CAR-T cells and general immune cells

In model (B.1), we extend the model presented in (4.10) by distinguishing between general immune cells and CAR-T cells. The outcome closely resembles what we observe in Figure A1(a): CAR-T cells initially reduce the cancer cell population rapidly, yet this effect is insufficient to raise the TCP curve above 0.6. We then proceed by combining virotherapy with CAR-T therapy. As shown in Figure A1(b), the TCP remains at zero when the two therapies are administered simultaneously. This outcome arises because the rapid action of oncolytic virotherapy eliminates cancer cells too quickly, limiting the opportunity for stimulation of CAR-T cell proliferation. By implementing our optimization strategy, which introduces a short delay in the administration of OVT, we allow CAR-T cells sufficient time to become effectively stimulated. Consequently, the virotherapy not only acts directly against cancer cells but also amplifies the cytotoxic response of CAR-T cells. In Figure A1(c), we observe that introducing just a one-day delay in virotherapy administration boosts the TCP value to 1.

Our general immune system consists of both tumor-specific and virus specific immune cells and, thus, will kill and be stimulated by both cancer cells and the virus. Our suggested extension of (2.1) is

$$\begin{aligned}
\frac{dC}{dt} &= rC\left(1-\frac{C+I}{L}\right)-\beta CV-\delta_T CT-\sigma VCT-p_2YC,\\
\frac{dI}{dt} &= \beta CV-\alpha I-\delta_T IT-\sigma VIT-q_2IY,\\
\frac{dV}{dt} &= \alpha bI-\omega V-\lambda VT-s_2VY+\tilde{u}(t),\\
\frac{dY}{dt} &= \eta YC+\zeta IY-\xi Y,\\
\frac{dT}{dt} &= \rho_2\left(C+I\right)T-\mu_2(C+I)T-\upsilon_2T.
\end{aligned} \tag{B.1}$$

In this model, we consider five cell populations: uninfected cancer cells (C), infected cancer cells (I), general immune cells (Y), CAR-T cells (T), and free viruses (V). The first four terms in equation one are similar to those in model (2.1), with the fifth term accounting for the killing of uninfected cancer cells by general immune cells at a rate of p_2. Similarly, in equation two, all terms except the fifth remain the same as in Eq (2.1), while the last term represents the killing of infected cells by immune cells at a rate of q_2. In equation three, the first two terms describe the effective replication of the virus and its clearance, respectively, while the third term accounts for the elimination of the OV by general immune cells at a rate of s_2. As before, $\tilde{u}(t)$ is the dimensional control term and has a similar definition as (4.4) after non-dimensionalization. Equation four remains identical to the immune cell equation in the base model (2.1). Finally, in equation five, the first term represents the stimulation and proliferation of CAR-T cells upon interaction with both infected and uninfected cancer cells at a rate of ρ_2. The second term denotes the inactivation of CAR-T cells by both tumor cell types at a rate of μ_2, while the last term represents their natural death at a rate of υ_2.

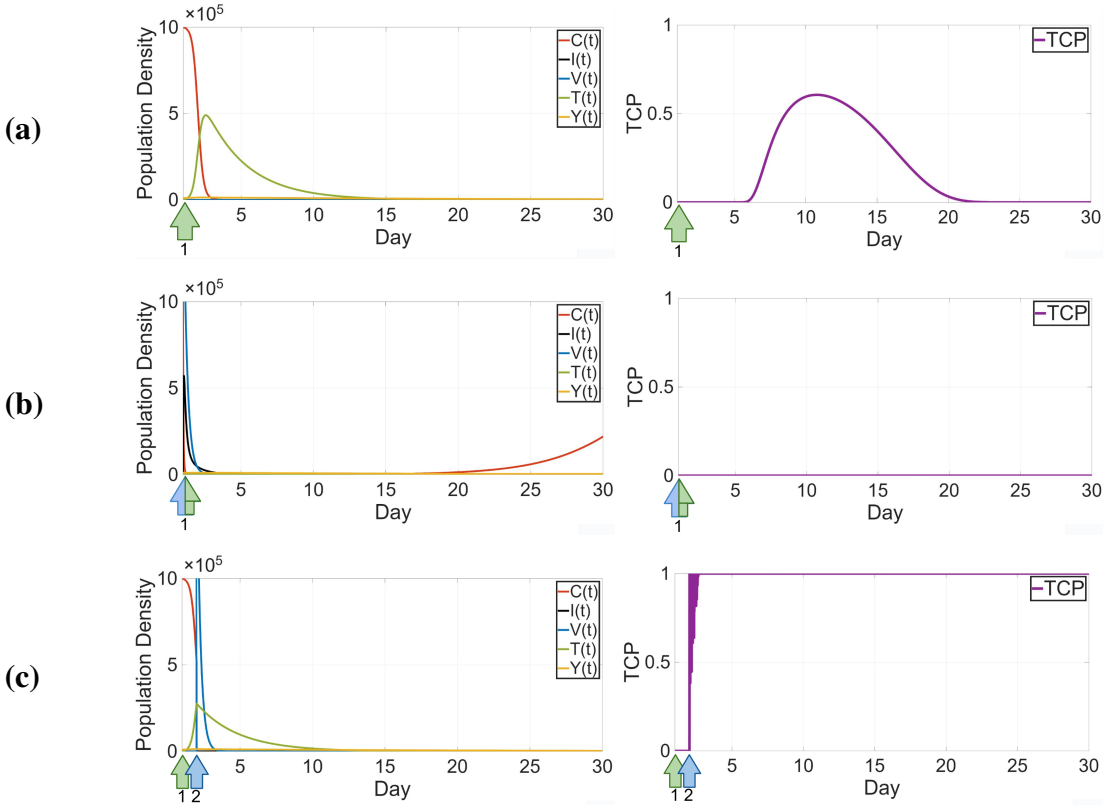

Figure A1. Dynamics of the cancer cells, immune cells, and CAR-T cells. The density of virus particles are re-scaled by dividing by 10^4 and CAR-T cells by 100. **(a)** No virus and injection of CAR-T cells on day one. **(b)** CAR-T cells and virus both on day one. **(c)** An optimized schedule with virus injection delayed to day two.

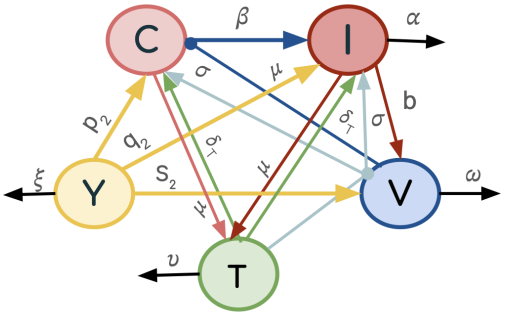

Figure A2. The blue arrows represent the viral infection of cancer cells at a rate β. The red arrow indicates the burst of viruses released from lysed infected cells at rate b. The light cyan arrows shows the virus-induced cancer cell killing of the CAR-T cells at the rate σ, while the orange arrows illustrate their direct killing of the cancer cells at the rate δ_T. The pink and red arrows denote the CAR-T cell death by the cancer cells at the rate μ. The interaction of general immune cells with uninfected cancer cells, infected cancer cells, and the virus is denoted in green arrows, and the immune cells kill them at the rate p_2, q_2, and s_2, respectively. All black arrows show cell death and virus degradation.

We see these interactions between the elements in Eq (B.1) more clearly in Figure A2. In this model, the similar parameters as in Eq (4.10) have the same values as in Table 4. The rest of parameters values are given in Table A2. We set the initial conditions to be

$$C(0) = 10^6, \quad I(0) = 0, \quad V(0) = 1.9 \times 10^{10}, \quad Y(0) = 10^4, \quad T(0) = 2 \times 10^6. \tag{B.2}$$

For choosing parameter values, since we are considering the innate immune system, we use the parameters from Al-Tuwairqi et al. [10] in this model as well and for the CAR-T therapy related parameters, we use the values from Barros et al. [38]. We again begin by applying CAR-T cell therapy alone. The simulation results are shown in Figure A1.

Table A2. Genreal immune cells and CAR-T cells model parameters, and their baseline values.

Parameter	Description	Baseline value	Units	Source
p_2	Killing rate of tumor cells by general immune cells	0.48×10^{-6}	$(\text{cell}\cdot\text{day})^{-1}$	[10] (estimated)
q_2	Killing rate of infected tumor cells by immune cells	0.63×10^{-6}	$(\text{cell}\cdot\text{day})^{-1}$	[10] (estimated)
s_2	Killing rate of virus by general immune cells	0.21×10^{-6}	$(\text{cell}\cdot\text{day})^{-1}$	[10] (estimated)
η_2	Stimulation of immune response by uninfected cells	3.84×10^{-7}	$(\text{cell}\cdot\text{day})^{-1}$	[10] (estimated)
ζ_2	Stimulation of immune response by infected cells	7.8×10^{-7}	$(\text{cell}\cdot\text{day})^{-1}$	[10] (estimated)
ξ_2	Clearance rate of general immune cells	0.036	$(\text{day})^{-1}$	[10]
ρ_2	CAR-T cells proliferation rate	4.5×10^{-6} $(2.3 \times 10^{-6}, 6 \times 10^{-6})$	$(\text{cell}\cdot\text{day})^{-1}$	[38]
μ_2	Immune cell exhaustion rate	1.24×10^{-8} $(1.24 \times 10^{-8}, 4.5 \times 10^{-8})$	$(\text{cell}\cdot\text{day})^{-1}$	[38]
υ_2	Natural death rate of immune cells	0.350 (0.350, 0.830)	$(\text{day})^{-1}$	[38]

B.2. Model with virus and cancer specific immune cells

Our next step to extend our results is making the immune response more specific. We assume that the T-cells are divided into two groups that primarily target either viral antigens or tumor antigens [52]. Thus, model (2.1) is extended to:

$$\begin{aligned}
\frac{dC}{dt} &= rC\left(1 - \frac{C - I}{L}\right) - \beta CV - pY_tC \\
\frac{dI}{dt} &= \beta CV - aI - q_tY_tI - q_vY_vI \\
\frac{dV}{dt} &= abI - \gamma V - sVY_v \\
\frac{dY_t}{dt} &= \eta Y_t(C + I) - \xi Y_t \\
\frac{dY_v}{dt} &= \zeta Y_vI - \nu Y_v.
\end{aligned} \tag{B.3}$$

The model now consists of five cell populations: the uninfected tumor cells (C), tumor cells infected with OVs (I) and tumor and virus specific T cells (Y_t) and (Y_v), respectively, and an OV population (V). Same as the base model (2.1), first term in equation one denotes the logistic growth of the uninfected cell in the absence of the treatment and the second term accounts for the infection of the cancer cells. The third term in this equation is describing the killing of the cancer cells by the tumor specific immune

cells at the rate of p. In the second equation, the first and the second term are similar to the base model describing the increase in the population of the infected cells and the death of such cells in the rate a, respectively. The infected cells are marked by the virus, so as we see the next two terms we have the death of the infected cells at the rate q_t by the tumor specific immune cells in the third term and also in fourth term their death at the rate q_v by the virus-specific T-cells. In the first term of equation three we have the effective replication of the virus by bursting out of the infected cell at rate b and their natural clearance at rate γ in the second term. The viruses are killed by the virus-specific immune cells at the rate s as described in the last term of equation three. The tumor-specific immune cells are stimulated by both infected and uninfected cancer cells. The first term of equation four denotes this stimulation at the rate η, andthe second term accounts for the clearance of this type of immune cells at the rate ξ. The first term of the last equation (B.3) accounts for the stimulation of the virus-specific immune cells at the rate ζ and the very last term describes their death the rate ν. We did not consider any clearance of the immune cells caused by the tumor cells. This was inspired by the model studied in [16]. In [16], K. Storey et al. incorporated both innate and adaptive immune responses in their virotherapy model. They further divided adaptive immune cells into antitumor and antiviral categories.

We see how the cancer cells, virus, and the immune cells interact with each other in Figure A3.

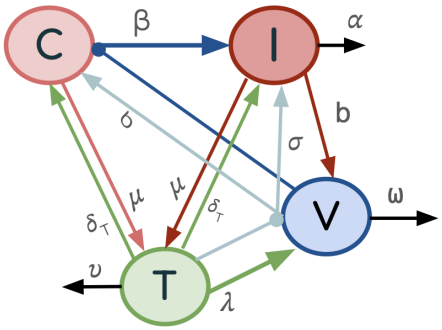

Figure A3. Interactions of the cancer cells, the oncolytic virus, and the virus and tumor specific immune cells.

We simulate the behavior of this model (figures not shown), and the parameter values are given in Table A3. We assume that at time t = 0 the tumor is at its maximum carrying capacity, with no infected cells. We also assume there is no virus specific immune cell before the injection as they get stimulated once the virus gets administered to the patient. The initial conditions of the system are

$$C(0) = L, \quad I(0) = 0 \quad V(0) = 1.9 \times 10^{10} \quad Y_t(0) = 10^4, \quad Y_v(0) = 0. \tag{B.4}$$

Parameter values were chosen similar to the model (2.1). We had to keep the values we had from Al-Twairqi et al. [10] for the immune stimulation related parameter values while for the clearance rate we could use a more specific value taken from Mahasa et al. [51]. The results are essentially the same as before, and we summarize those in Table A4.

Table A3. Immune specific model parameters, and their baseline values.

Parameter	Description	Baseline value	Units	Source
r	Growth rate of uninfected tumor cells	0.3	$(\text{day})^{-1}$	[9]
L	Tumor carrying capacity	10^6 ($10^6 - 10^8$)	cells	[9]
β	Infection rate of uninfected tumor cells by free viruses	1.5×10^{-9}	$(\text{virus}\cdot\text{day})^{-1}$	[9]
p	Killing rate of tumor cells by tumor-specific immune cells	0.48×10^{-6}	$(\text{cell}\cdot\text{day})^{-1}$	[10] (estimated)
r	Death rate of infected tumor cells	1	$(\text{day})^{-1}$	[9]
q_t	Killing rate of infected tumor cells by tumor-specific immune cells	0.63×10^{-6}	$(\text{cell}\cdot\text{day})^{-1}$	[10] (estimated)
q_v	Killing rate of infected tumor cells by virus-specific immune cells	0.63×10^{-6}	$(\text{cell}\cdot\text{day})^{-1}$	[10] (estimated)
b	Viruses released by lysed infected tumor cell	3500	$(\text{virus})(\text{cell})^{-1}$	[9]
γ	Virus-induced immune response rate	4	$(\text{day})^{-1}$	[9]
s	Killing rate of virus by virus-specific immune cells	0.21×10^{-6}	$(\text{cell}\cdot\text{day})^{-1}$	[10] (estimated)
η	Stimulation of immune response by uninfected cells	3.84×10^{-7}	$(\text{cell}\cdot\text{day})^{-1}$	[10] (estimated)
ζ	Stimulation of immune response by infected cells	7.8×10^{-7}	$(\text{cell}\cdot\text{day})^{-1}$	[10] (estimated)
ξ	clearance rate of tumor-specific immune cells	0.009	$(\text{day})^{-1}$	[51]
ν	clearance rate of virus-specific immune cells	0.1329	$(\text{day})^{-1}$	[51]

Table A4. Summary of treatment strategies, schedules, viral doses, and TCP outcomes for model (B.3). The most promising scenarios are shown in bold.

Strategy	Treatment week (s)	Treatment schedule (Days)	Total dose	Max TCP
(S1) Increasing θ	Week 1	Day 1	95	0
	Week 1	Day 1	95	0.39
	Week 1	**Day 1**	**95**	**0.96**
(S2) Optimized OVT schedule	Week 1	Days 1, 3, 5	95	0
	Weeks 1, 2	Days 1, 5, 11	190	0.53
	Weeks 1–3	**Days 1, 8, 9, 15, 16**	**285**	**0.99**
	Weeks 1, 2, 4	**Days 1, 8, 9, 22**	**285**	**0.97**
	Weeks 1, 3, 4	**Days 1, 15, 16, 22, 23**	**285**	**0.96**
Combination therapies				
(S3a) Immunosuppression (ϵ_t)	Week 1	Day 1 ($\epsilon_t = 0.25$)	95	0
	Week 1	Day 1 ($\epsilon_t = 0.5$)	95	0
	Week 1	Day 1 ($\epsilon_t = 0.75$)	95	0
(S3b) Immunostimulation ($\chi = 2.5$)	Week 1	Day 1	95	0
(S3c) CAR-T therapies	Week 1	CAR-T: Day 1	CAR-T: 0.2	0
	Week 1	**CAR-T: Day 1; OV: Day 1**	**CAR-T: 0.2; OV: 95**	**0.99**